

EQUILIBRIUM AND TRANSIENT PYRIDINE POISONING
OF A HYDROTREATING CATALYST

By

JEFFREY ALAN KITTRELL

Bachelor of Science

Michigan State University

East Lansing, Michigan

1984

Submitted to the Faculty of the
Graduate College of the
Oklahoma State University
in partial fulfillment of
the requirements for
the Degree of
MASTER OF SCIENCE
May, 1986

Thesis
1986
Klode
cop. 2



EQUILIBRIUM AND TRANSIENT PYRIDINE POISONING
OF A HYDROTREATING CATALYST

Thesis approved:

Mayis Seapan

Thesis Adviser

Billy L. Cyres

Harry L. Fentel

Norman M. Durham

Dean of the Graduate College

1251284 |

ABSTRACT

An investigation was conducted on the adsorption of pyridine on a NiMo/Al₂O₃ (Shell 324) hydrotreating catalyst. Equilibrium and transient adsorption data were collected at 250°C, 350°C, and 450°C in the pyridine partial pressure range of 284 N/m²-2130 N/m² (11 wt%-30 wt%). The equilibrium adsorption isotherms demonstrated idealized Langmuir characteristics (Type I isotherm behavior). The partial pressure independent equilibrium values (at 250°C, 350°C, and 450°C) demonstrated a linear temperature dependence. No systematic trend was found between the transient adsorption data and pyridine partial pressure. However, as the adsorption temperature was decreased the rate of adsorption increased. Pyridine adsorption at 450°C demonstrated a 33% irreversibility which is attributed to coke formation. Two mathematical models were developed which accurately predicted the transient adsorption data. The first model predicted the period when reversible pyridine adsorption and irreversible coke formation were simultaneously poisoning the fresh catalyst. The second model predicted the period when coke formation had reached a steady-state level and only reversible pyridine adsorption was occurring on the catalyst surface. The model parameters for these exponential expressions are functions of pyridine partial pressure and rate constants for adsorption, desorption, and coke formation. Additional experimentation was completed to study catalyst reduction. The oxidic catalyst was reduced when exposed to hydrogen or ammonia (in the same temperature and partial pressure range as that of pyridine).

ACKNOWLEDGEMENT

I wish to express my sincere gratitude and appreciation to my major advisor, Dr. Mayis Seapan, for his many valuable suggestions, guidance, and confidence in my work. I would also like to thank Dr. Gary Foutch and Dr. Billy Crynes as members of my examining committee.

My appreciation is due to the Oklahoma State University, School of Chemical Engineering, and the University Center for Energy Research (UCER) for providing a very generous supply of facilities, materials, and financial support. My appreciation is also due to Amoco Oil Company for providing me with a Master's Fellowship.

I am very grateful to Pamela Hartman for her patience and dedication in typing this manuscript.

I would like to acknowledge my two very good friends, Mike Haroun and Bill Vedder. We have spent many hours together during the last one and one-half years and have grown to be close friends. The time I have spent here in Stillwater has been very enjoyable and I will always remember my friendship with these two gentlemen.

Finally, I would like to thank my entire family for their love and support throughout my educational career. I wish to acknowledge my loving wife, Susan, who has spent endless hours studying with me, supporting me, and giving me the motivation to succeed not only in graduate school, but at Michigan State as well. I wish to express my love and appreciation to my parents who have also supported me in everything I chose to do.

This thesis is dedicated to my father, Dr. James Raymond Kittrell, who has taught me so many valuable lessons during my education, but more importantly about life in general, and whom I hold with the utmost respect.

TABLE OF CONTENTS

Chapter	Page
I. INTRODUCTION.....	1
II. LITERATURE REVIEW.....	4
III. EXPERIMENTAL EQUIPMENT AND PROCEDURE.....	16
Equipment.....	16
Procedure.....	19
IV. EXPERIMENTAL RESULTS.....	22
V. DISCUSSION.....	37
VI. CONCLUSIONS AND RECOMMENDATIONS.....	68
BIBLIOGRAPHY.....	71
APPENDIX A - BUOYANCY CALCULATIONS.....	73
APPENDIX B - PROGRESSIVE SHELL MODEL DERIVATION.....	79
APPENDIX C - REDUCTION CALCULATIONS.....	84

LIST OF TABLES

Table		Page
I.	Heterocyclic Nitrogen Compounds Found in Coal-Derived Liquids.....	2
II.	Properties of Shell 324 Catalyst.....	20
III.	Pyridine Equilibrium Adsorption Data.....	23
IV.	Transient Adsorption Data.....	27
V.	Catalyst Reduction Data.....	32
VI.	Pyridine Adsorption/Desorption Data.....	35
VII.	Catalyst Coke Content Data.....	54
VIII.	Reversible Poisoning and Irreversible Coking Model Parameters.....	59
IX.	Buoyancy Changes in Equilibrium Pyridine Adsorption Data.....	77

LIST OF FIGURES

Figure	Page
1. Schematic Flow Diagram of Experimental System.....	17
2. Equilibrium Adsorption Isotherms for Pyridine.....	25
3. Transient Pyridine Adsorption Behavior.....	31
4. Catalyst Reduction Behavior Due to Hydrogen and Ammonia Adsorption.....	33
5. Pyridine Adsorption Reversibility Behavior.....	36
6. Equilibrium Adsorption Weight Dependence on Temperature.....	41
7. Reversible Poisoning Model Log Plot of Run 17 Transient Data.....	45
8. Run 17 Transient Adsorption Data Prediction from Reversible Poisoning Model.....	47
9. Reversible Poisoning Model Log Plot of Run 17 and 23 Transient Data.....	53
10. Run 17 Transient Adsorption Data Prediction from Reversible Poisoning and Irreversible Coking Models.....	60
11. Run 22 Transient Adsorption Data Prediction from Reversible Poisoning and Irreversible Coking Models.....	61
12. Run 23 Transient Adsorption Data Prediction from Reversible Poisoning and Irreversible Coking Models.....	62
13. Run 24 Transient Adsorption Data Prediction from Reversible Poisoning and Irreversible Coking Models.....	63
14. Run 15 Transient Adsorption Data Prediction from Reversible Poisoning Model.....	64
15. Run 25 Transient Adsorption Data Prediction from Reversible Poisoning Model.....	65
16. Run 17 Transient Adsorption Data Prediction from Progressive Shell Model.....	82

CHAPTER I

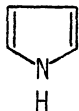
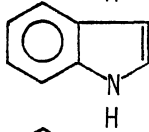
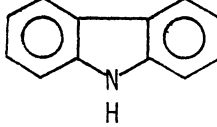
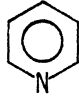
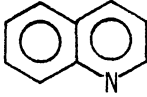
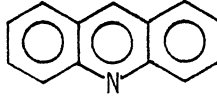
INTRODUCTION

Sources of high quality crude oils are on the decline. As such, refiners are having to process heavy oil fractions which contain high concentrations of aromatic or cyclic amines. In addition, alternative energy resources are being developed, such as shale oil processing or coal liquefaction, which contain significant amounts of nitrogenous heterocyclic compounds.

Nitrogen compounds are undesirable in any petroleum liquid for several reasons. Gums and precipitates form during the storage of high nitrogen content oils. The combustion of high nitrogen content oils and fuels contributes to NO_x emissions. The activity of catalysts used in refining processes, such as cracking, reforming or hydrotreatment, is reduced if the feedstocks contain nitrogen compounds. Coal-derived liquids are believed to be carcinogenic mainly due to the presence of heterocyclic nitrogen compounds.

One of the simplest compounds typically found in high nitrogen content petroleum liquids is pyridine. This compound contains only one ring and has relatively few hydrogenation derivatives. Due to this simplicity, pyridine is often chosen as a model compound for study in petroleum liquid research. A brief list of typical basic and nonbasic nitrogen compounds found in petroleum liquids is shown in Table I.

TABLE I
 HETEROCYCLIC NITROGEN COMPOUNDS FOUND
 IN COAL-DERIVED LIQUIDS

Name	Formula	Structure	Basic
Pyrrole	C_4H_5N		No
Indole	C_8H_7N		No
Carbazole	$C_{12}H_9N$		No
Pyridine	C_5H_5N		Yes
Quinoline	C_9H_7N		Yes
Acridine	$C_{13}H_9N$		Yes

A popular method to remove nitrogen compounds from petroleum liquids is called hydrodenitrogenation (HDN). It is generally believed that HDN occurs through hydrogen saturation of the heterocyclic ring followed by ring fracture to eventually form ammonia. The problem with this process, however, is that the intermediate basic nitrogen compounds also act as poisons to the acidic hydrotreating catalyst.

The purpose of this study is to investigate the poisoning of a hydrotreating catalyst by model nitrogen compounds, pyridine and ammonia. Furthermore, the phenomenon of carbonaceous deposit (coke) formation will be briefly studied and modeled. The specific objectives of this study are as follows:

- 1) to study the adsorption (transient and equilibrium values) of individual model nitrogen compounds - pyridine and ammonia - on a typical hydrotreating catalyst;
- 2) to investigate the formation of carbonaceous deposits on a hydrotreating catalyst during the adsorption of carbon containing nitrogen compounds;
- 3) to model the catalyst poisoning process (including nitrogen compound adsorption and coke formation).

CHAPTER II

LITERATURE REVIEW

There have been many studies which were concerned with the nature of acidic sites on a particular catalyst. Tanabe (1) has suggested that there are different types of acidic sites on catalyst surfaces, some behaving as stronger acids than others. At elevated temperatures, adsorbed bases will preferentially evacuate weak acidic sites before evacuating stronger sites. Thus, the proportion of adsorbed base which is evacuated at various temperatures may give an indication of the acid strength.

There are two types of acidic sites which exist on a cracking catalyst, Brønsted and Lewis acid sites. Brønsted acid sites are capable of donating a proton to a base. Lewis acid sites can accept unpaired electrons from a base (2). The utilization of infrared spectroscopy has allowed these two types of sites to be differentiated. Basic molecules, such as ammonia and pyridine, have the property that their interaction with Brønsted and Lewis acid sites produce different species detectable by infrared spectroscopy. Ward (3) has found that adsorption on Brønsted acid sites by ammonia, pyridine, and piperidine produces ammonium, pyridinium, and piperidinium ions with characteristic frequencies of 1475, 1545, and 1610 cm^{-1} respectively. Ward (3) has also reported that adsorption on Lewis acid sites produces corresponding bands near 1630, 1450, and 1450 cm^{-1} .

Maxted (4) was the first to discover, in the early 1950s, the relation between the acidic characteristics of catalysts and their hydrogenation and cracking activity. Maxted concluded that a particular molecule poisons a catalyst due to it containing unshared external electron pairs which enable a strong chemisorptive bond to occur between the catalyst and the molecule. Maxted also found that the degree of poisoning of the catalyst increased with the molecular size of the poison and with the strength of the bond between the catalyst and the poison.

It is quite common in catalyst manufacture to place active species or reaction promoters on an inert support material. This support may be any of a number of materials but a common support is alumina. In 1959 Pines and Haag (5) investigated the possibility that alumina had an intrinsic acidity. They proposed that the catalyst acidity of alumina could be due to either Brønsted or Lewis acid sites. After completion of various chemical indicator tests it was found that the alumina tested positive for acidity and these acid sites could only be Lewis acid sites. Brønsted sites, if present at all, were of very low acid strength.

In this same study, Pines and Haag (5) also investigated the effect of calcination temperature on alumina. Based on the results of the isomerization of cyclohexene to methylcyclopentene, it was found that the maximum catalytic activity of alumina occurred when the sample was calcined between 600°C-700°C. The high activity seemed to be associated with an alumina surface which was partially covered with water. At a 600°C calcination temperature, the fraction of the alumina surface which was covered with water (in the form of hydroxyl groups) was 0.54.

There have been many studies conducted on catalyst poisoning due to nitrogen compounds. In 1950, Mills, Boedeker, and Oblad (6) studied the poisoning of cracking catalysts by nitrogen compounds. In this study a sensitive direct weighing technique was developed for determining the amount of quinoline or pyridine adsorbed by the catalysts ($\text{SiO}_2\text{-Al}_2\text{O}_3$). The organic nitrogen bases were found to be held by both physical and chemical forces on the catalyst surface. Furthermore, the catalyst which had been exposed to quinoline adsorption, below 425°C , remained a pale green color. Further analysis confirmed that quinoline was indeed held on the catalyst surface rather than its decomposed or polymerized product at cracking conditions. Quinoline slowly decomposed to a polymerized product (coke) above 425°C .

In addition to studying adsorption of basic compounds, Mills et al. (6) also found a relation between amount of base adsorbed and fraction of catalyst surface covered by active sites. Assuming a flat-lying quinoline molecule covers 36 \AA^2 of surface area, only about 4% of the catalyst surface was covered by quinoline. Thus, a major part of the catalyst surface does not contribute to the cracking activity of the catalyst.

Hirschler (7) found that adsorption of quinoline does not deactivate all the active catalyst sites. Chemisorbed quinoline only causes a modest reduction in the total number of active sites and strongly modifies the acid strength distribution. The difference between Hirschler's and Mills' conclusions were that Mills believed all active acid catalyst sites were covered by quinoline. However, Hirschler believed that the majority of the catalyst surface was made up

of low strength acid sites and the adsorbed quinoline only covered the strong acid sites.

In 1976 Takahashi et al. (8) conducted a study on the nature of adsorbed sites on catalysts. They investigated the behavior of pyridine on a silica-alumina catalyst with a thermal desorption method. Since pyridine has a rather low basicity ($pK_a = 5.18$), the information of stronger acid sites on the surface could be obtained. It was found that the stronger acid sites on the silica-alumina were distributed in different acid strengths. Furthermore, the ratio of Lewis acid sites to Brønsted acid sites was about 2.9 - 6.0 in some kinds of silica-alumina.

In 1978 Cowley and Massoth (9) investigated pyridine poisoning of a sulfided Mo- Al_2O_3 catalyst. They found that pyridine adsorbs on active desulfurization sites. The amount of pyridine which was required to produce a fully poisoned catalyst (zero activity) was 0.24 molecules of pyridine per molybdenum atom. However, there was an uncertainty that each adsorbed molecule was effective in poisoning a catalytically active site. Therefore, the value obtained (0.24 molecules pyridine/molybdenum atom) for active sites should be considered a maximum one.

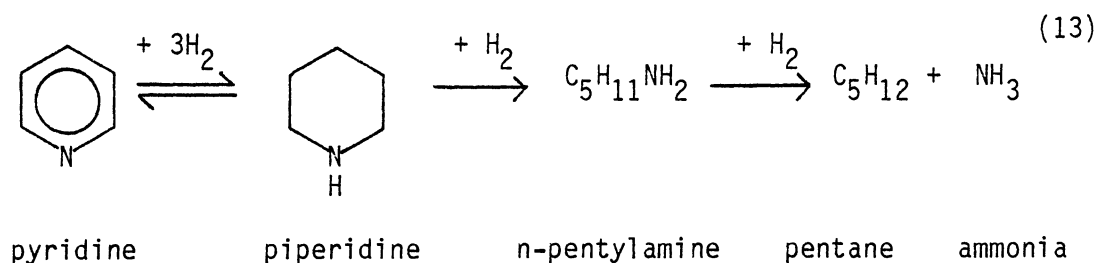
In 1982, Ramachandram and Massoth (10) studied the nature of active sites of aged and pyridine poisoned Mo- Al_2O_3 and CoMo- Al_2O_3 catalysts. They found that deactivation via coking or poisoning only reduces the number of active sites but does not alter the remaining sites.

In 1984 Hall et al. (11) investigated the site selective adsorption of nitrogen compounds on sulfided Mo- Al_2O_3 catalysts. Although pyridine did adsorb on and poison the active catalytic sites of molybdenum, a majority of the pyridine adsorption occurred on the alumina surface.

Ammonia, like pyridine, was also found to adsorb unselectively on both the alumina and molybdenum active sites.

It has been reported by Tanabe (1) that methods which utilize adsorption and desorption in the gaseous phase have the advantage that a catalyst may be studied under its actual working conditions (several hundred degrees centigrade). However, this type of analysis has the disadvantage that it is difficult to distinguish between physical and chemical adsorption.

In addition to the many studies on the nature of catalyst active sites and nitrogen poisoning of these sites, there have also been a significant number of studies pertaining to hydrodenitrogenation. In 1971 McIlvried (12) studied the kinetics of the hydrodenitrification of pyridine. McIlvried found that pyridine denitrification proceeds by rapid hydrogenation of pyridine to form piperidine, slow ring rupture to form n-pentylamine, and rapid denitrification of n-pentylamine to form ammonia. Schematically this may be demonstrated by:



McIlvried (12) also found that only ammonia appeared to be adsorbed on the metallic dehydrogenation sites. However, all the nitrogen compounds appeared to be equally distributed on the denitrification sites.

In 1975 Satterfield and Cocchetto (14) published a paper concerning what they believed to be an equilibrium limitation on the formation of piperidine during pyridine hydrogenation. They found that pyridine conversion goes through a maximum at about 380°C due to thermodynamic limitations on the first step of the denitrification mechanism. Above 380°C, equilibrium was found to shift in favor of pyridine rather than piperidine. This resulted in reducing the hydrogenolysis of the C-N bond (piperidine → n-pentylamine) because of a lack of piperidine reactant. Thus, pyridine conversion was reduced.

Entz (13) studied the adsorption of pyridine and its hydrogenation intermediates on a NiMo/Al₂O₃ hydrotreating catalyst. Entz found that pyridine was not completely converted to pentane and ammonia at 400°C and that the hydrogenation intermediates were irreversibly adsorbed on the catalyst. The adsorption of hydrogen and the effects of catalyst poisoning on hydrogen adsorption were also investigated. Ammonia reduced hydrogen adsorption by 29% and n-pentylamine reduced hydrogen adsorption by 47%. The irreversibly adsorbed compounds resulting from piperidine and pyridine hydrogenation reduced hydrogen adsorption by 44% and 41% respectively.

It is a common fact that organosulfur compounds are found with organonitrogen compounds in low quality petroleum stocks. The inhibiting effect of organonitrogen compounds on catalytic hydrodesulfurization (HDS) has already been established. However, little has

been published on the effects of organosulfur compounds on hydrodenitrogenation (HDN). In 1975 Satterfield et al. (15) published a paper dealing with the interactions between HDS and HDN. It was found that sulfur compounds have two effects on HDN. At low temperatures ($\sim 200^{\circ}\text{C}$), they compete with pyridine for hydrogenation sites and thus inhibit the rate of hydrogenation of pyridine in the denitrification mechanism. At high temperatures ($\sim 400^{\circ}\text{C}$) the HDS reaction product, hydrogen sulfide, interacts with the catalyst to improve the hydrogenolysis activity.

The effect of sulfur and catalyst sulfidation are quite important in HDN. Shih et al. (16) found that presulfiding an HDN catalyst greatly improved the total nitrogen removal rate. Presulfidation was determined to increase the rate of hydrogenation while not affecting the hydrogenolysis step. However, the presence of hydrogen sulfide, the end product of the HDS reactions, increases the total nitrogen removal by enhancing the hydrogenolysis step.

Goudriaan et al. (17) published some very interesting quantitative data concerning the effects of sulfur on HDN. The temperature required to attain a certain degree of nitrogen removal is 25°C lower with a presulfided catalyst than with the catalyst in its oxidic state. The presence of hydrogen sulfide during HDN further reduces this temperature by 60°C . Pyridine ring hydrogenation is 25-45% higher on a presulfided catalyst than on the oxidic catalyst. The hydrogenolysis reaction is 5-15% higher between $250\text{-}350^{\circ}\text{C}$ for a presulfided catalyst than with the oxidic catalyst. The presence of hydrogen sulfide increases this conversion by another 20-50%.

Catalyst components also affect the degree of HDN. Thakkar et al. (18) have found that catalysts containing Ni-Mo had the highest HDN activity. The next best catalysts contained Co-Mo, and the least effective HDN catalyst contained Ni-W. NiMo/Al₂O₃ catalysts demonstrated 68% nitrogen removal, CoMo/Al₂O₃ catalysts demonstrated 51% nitrogen removal, and NiW/Al₂O₃ catalysts demonstrated 10% nitrogen removal. Desulfurization for all the above catalysts was consistently high, ranging from 85 to 100%. This substantiates observations that nitrogen removal is more difficult than sulfur removal.

An additional problem which may occur when nitrogen bases poison a catalyst surface is the phenomenon of carbonaceous deposit formation or coke formation. Fu and Schaffer (2) suggested that nitrogen bases only poison acidic sites and not the metal sites responsible for hydrogen production. In the absence of hydrogen then, dehydrogenation of an organic nitrogen compound by active metal sites may induce very rapid carbon polymerization (coke formation) at appropriate temperatures (> 425°C). Coke has also been found to form during HDN reactions, but in the presence of hydrogen coke formation is significantly reduced.

There have been many attempts to relate catalyst activity to coke content. Anderson and Whitehouse (19) proposed four equations which could be used to relate catalyst activity to coke content. These equations were not concerned with phenomena within a catalyst particle but more with the bulk behavior of a catalyst bed.

Ozawa and Bischoff (20) developed empirical relationships between catalyst activity and coke content based on the kinetics of coke formation reactions during the cracking of ethylene over a silica-alumina catalyst. With the use of a thermogravimetric system, Ozawa and

Bischoff found a linear function described the decline of catalyst activity with coke level, except for the initial period of very rapid activity decline. The rate constant for the coke formation reaction was found to exhibit an exponential relationship.

Dumez and Froment (21) studied the kinetics of 1-butene dehydrogenation over a $\text{Cr}_2\text{O}_3\text{-Al}_2\text{O}_3$ catalyst. They proposed an exponential relationship to describe the catalyst activity - coke content data. Dumez and Froment reported hydrogen had an inhibiting effect on coke formation. They also reported that their model parameter did not exhibit a systematic trend with respect to the temperature or partial pressure of the feed.

There are three conventional regimes of hydrocracking catalyst behavior; fouling due to nitrogen base adsorption on acidic catalyst sites, a linear regime due to slow coking, and a regime of accelerated coking characterized by an exponential increase in temperature with time. Krishnaswamy and Kittrell (22) have developed an n^{th} order, concentration independent deactivation model which predicts the time-temperature relationship required to maintain constant conversion of reactant. Both the linear and exponential regimes of the temperature-time curve are well described by the model.

Romero et al. (23) have presented an equation, based on the conversion of benzyl alcohol to benzaldehyde, representing the deactivation of a Cu-SiO_2 catalyst. They proposed a kinetic scheme where deactivation (coke formation) takes place in parallel with the main reaction. This type of kinetic analysis allows simultaneous deactivation mechanisms to be modeled.

Nam and Kittrell (24) have developed a model which makes use of an active site balance concept to relate catalyst activity to catalyst coke content. The deactivation model described data represented by a linear dependence (Ozawa and Bischoff (20)), an exponential dependence (Dumez and Froment (21)), and a hyperbolic dependence (Takeuch et al. (25)).

Chang et al. (26) have developed an empirical model to describe parallel fouling of a hydrotreating catalyst. Experimentation was based on hydrotreatment of a 30 wt% SRC feedstock in a trickle-bed reactor which contained a NiMo-Al₂O₃ catalyst. The model accurately predicted coke profiles as a function of time and reactor position. The model also predicted hydrogenation and hydrodenitrogenation as functions of catalyst coke content.

There has been quite a bit of work done in the areas of catalyst surface acidity, poisoning, hydrotreating, and coking. There are two types of acidic sites on a catalyst surface, Brønsted acid and Lewis acid sites. The utilization of infrared spectroscopy has allowed the proportion of these sites on a catalyst surface to be distinguished. Furthermore, the activity of catalysts are proportional to their ability to adsorb basic nitrogen compounds on these acidic sites. Chemisorption of a nitrogen base on a catalyst surface causes a modest reduction in the total number of active sites and strongly modifies the active strength distribution.

During nitrogen compound poisoning of catalysts, organic bases are held on the catalyst surface by both physical and chemical forces. A majority of the pyridine which poisons a Mo/Al₂O₃ catalyst will adsorb on the alumina surface rather than the molybdenum surface. During the

poisoning of a sulfided catalyst nitrogen bases will adsorb on active desulfurization sites.

Hydrodenitrogenation studies were also investigated and a NiMo/Al₂O₃ catalyst was generally more active for HDN than a CoMo/Al₂O₃ or NiW/Al₂O₃ catalyst. It is believed that a thermodynamic limitation in the pyridine hydrogenation step of pyridine HDN occurs at about 380°C. Presulfidation of an HDN catalyst increases the rate of hydrogenation in HDN and thus increases the conversion (nitrogen removal). However, the presence of sulfur (in the form of H₂S) does not affect hydrogenation but does enhance hydrogenolysis of the C-N bond (piperidine → n-pentylamine) and increases nitrogen removal.

Another problem found to occur during nitrogen base poisoning was coke formation which was a significant problem above 425°C. There have been many relations between catalyst activity and coke content. These developed relationships were both empirical and theoretical and described linear, exponential, or hyperbolic behavior. The advantage of using kinetic, time-dependent models is that simultaneous poisoning mechanisms may be described (e.g. basic nitrogen poisoning with simultaneous coke formation).

With the abundance of nitrogen poisoning and coke formation studies which exist, very few if any have attempted to simplify the poisoning mechanism for study. In terms of nitrogen base poisoning there has been very little work completed on investigating equilibrium adsorption as a function of temperature and pressure (adsorption isotherms). Furthermore, very little work has been completed on modeling the transient poisoning data which arises from any equilibrium study. In addition, the experimental coking studies have mainly focused on the

effect of coke formation on catalyst activity for a particular reaction system. There seems to be little information on simultaneous coke formation and nitrogen compound adsorption.

The purpose of this study is to investigate adsorption of particular model nitrogen bases on a typical hydrotreating catalyst. The equilibrium data will be investigated and compared to theoretical developments (i.e. Langmuir Theory). In addition, the kinetics of the poisoning mechanism will be studied and a relationship between nitrogen base poisoning and coke formation will be developed. This relationship will be used to predict the transient adsorption data.

CHAPTER III

EXPERIMENTAL EQUIPMENT AND PROCEDURE

Equipment

A schematic flow diagram of the experimental system is shown in Figure 1. A Cahn System 113 Thermal Gravimetric Analyzer (TGA) was used for measurement of model compound adsorption on the catalyst surface. The TGA apparatus consists of a null beam type electrobalance which measures weight changes of a catalyst pellet suspended in a temperature controlled gas stream. The microbalance has a maximum sample limit of 2.5 grams and can detect weight changes as small as 0.1 micrograms. The concept behind the microbalance is that it converts weight changes to electrical signals which can be recorded on a strip chart recorder.

The Cahn System 113 also includes a Micricon programmer/controller. The programmer allows a temperature/time profile to be followed by the furnace. The controller is a proportional-integral-derivative (PID) controller which is capable of raising the furnace temperature at a rate between 0 and 5°C/minute up to a maximum temperature of 1150°C.

The Cahn System 113 also contains a strip chart recorder component system which includes time derivative computer (TDC) and automatic range expander/percent sample weight accessories. The time derivative computer converts the direct weight change signal to a rate of weight change with respect to time signal. The automatic range expander

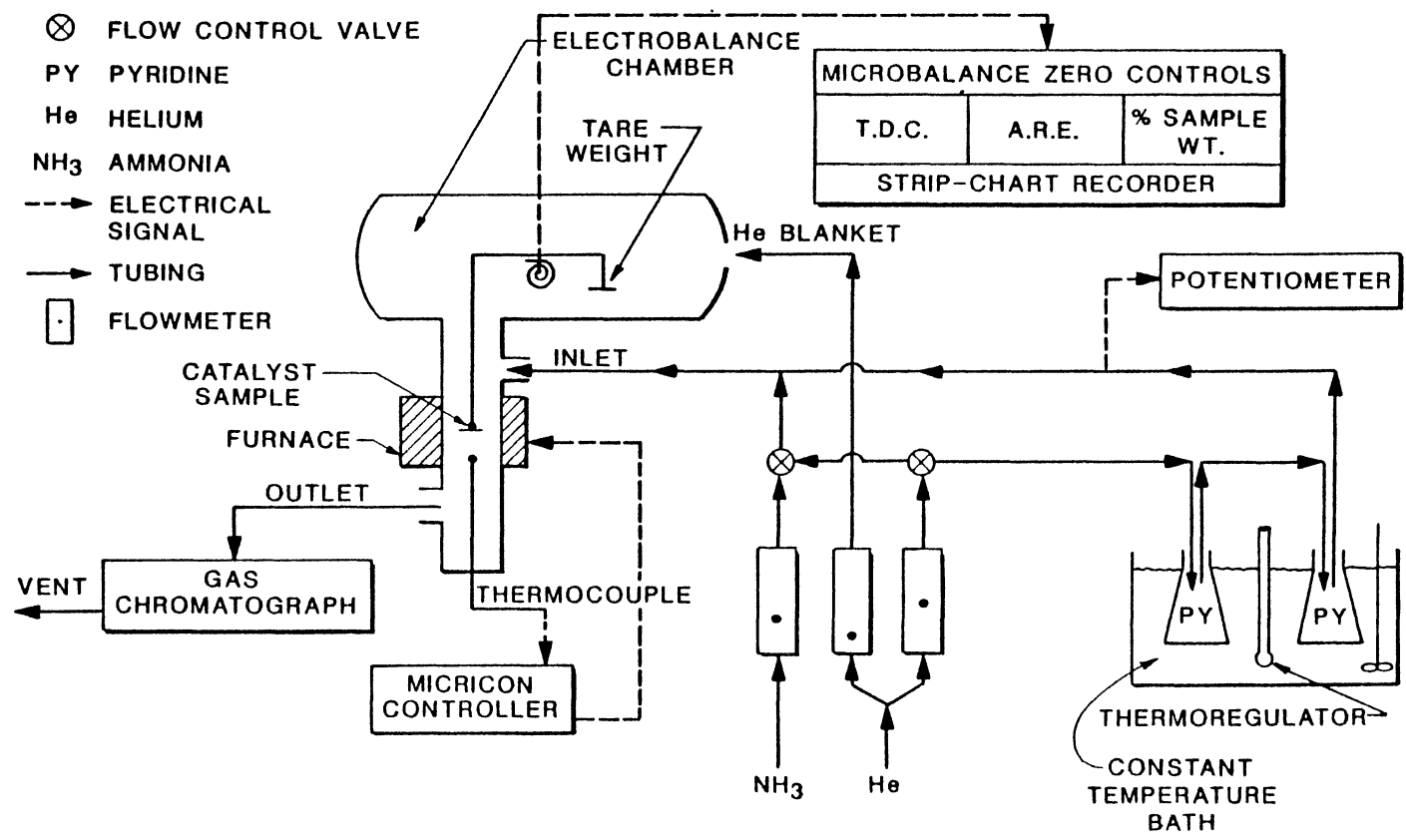


Figure 1. Schematic Flow Diagram of Experimental System

maintains the signal output between two fixed limits, and the percent sample weight accessory displays the signal output as a percentage of the weight loss or gain. However, the TDC and range expander/percent sample weight accessories were not used in the present experimentation.

Supplemental equipment included a porosimeter, constant temperature water bath, and gas chromatograph. A Quantachrome SP-10B Scanning Porosimeter was used to determine catalyst pore volume, pore distribution, and surface area. The procedure consisted of forcing mercury into an evacuated catalyst sample with pressure and measuring the change in volume of the mercury.

A Precision (Model 666000) Differential Thermometer and Thermoregulator was used to maintain a constant temperature water bath. This constant temperature bath was used to maintain pyridine at a constant temperature during the saturation of a helium stream. Two 500 ml filter flasks were arranged in series and contained 500 ml of liquid pyridine. Ultra-high purity helium (99.999%) flowed through gas dispersion tubes and into the constant temperature pyridine. Pyridine/helium vapor then flowed out of the last saturator and through a heated line to the TGA. The heated tube was maintained at 100°C by heating tapes. Heated tubing temperature was monitored by a Leeds & Northrup Model 8686 millivolt potentiometer.

After entering the TGA, the pyridine/helium vapor flowed down over a suspended catalyst pellet. After passing over the catalyst, the pyridine/helium vapor exited a vent port and flowed through another heated line to a Varian (Model 3700) gas chromatograph. The gas chromatograph was used to determine the partial pressure of pyridine in the helium stream. For resolution and analysis of C_5H_5N (pyridine), a

3.175 mm x 1.52 m (1/8 in x 5 ft) stainless steel column of 10% Carbowax 20 M on 80/100 mesh Chromosorb W-HP was used.

The method of ammonia saturation was slightly different. Ultra-high purity ammonia was mixed with ultra-high purity helium in appropriate ratios to correspond to identical pyridine in helium concentrations. This gas mixture was then sent to the entrance port on the TGA. Matheson flowmeters were used to obtain accurate flow ratios. A Matheson 7642T flowmeter was used to regulate helium flow. A Matheson 7642T flowmeter with Burma seals was used for the highly corrosive ammonia environment.

Procedure

The Shell 324 ($\text{NiMo}/\text{Al}_2\text{O}_3$) HDN catalyst was used for study during this experimentation. The properties of this catalyst are shown in Table II. One extrudate pellet (approximately 10 mg mass) was used per run. Each pellet was placed in a nickel-chromium alloy basket inside the TGA hangdown tube. The pellet was then heated to 500°C at a rate of 1.39°C/min (six hours) while exposed to a 10 cm³/min flow of zero-grade (3 ppm H₂O) air. The temperature was then maintained at 500°C for 12 hours. At the end of this time, the temperature was lowered to 450°C at a rate of 0.42°C/min (2 hours). The catalyst was then dried in ultra-high purity (UHP) helium until a constant weight was achieved.

When a constant catalyst weight was achieved, UHP helium was sent through the pyridine saturators, through heated (100°C) tubing, and into the TGA. The helium flow rate through the saturators was 82 cm³/min and a 10 cm³/min helium blanket flowed through the electrobalance chamber. Pyridine/helium flow was maintained at constant furnace temperature

TABLE II
PROPERTIES OF SHELL 324 CATALYST

Shape	Extrudate
Nominal size, mm	1.6*
Metals Content, wt%	
Nickel	2.67*
Molybdenum	13.05*
Physical Properties	
Surface Area, m ² /kg cat. (x 10 ⁻³)	208
Total Pore Volume, m ³ /kg cat. (x 10 ³)	0.54
Pore Distribution (most frequent diameter), nm	5.4

* Vendor's data

until a constant catalyst adsorption weight was reached. Constant weight was designated as the point at which less than one microgram of poison adsorbed on the catalyst surface during a 2-4 hour period. At this point the furnace temperature decreased to 350°C at a rate of 0.42°C/min. Pyridine/helium flow was maintained during the temperature change and when steady-state weight was reached the procedure was repeated with the exception of temperature being changed to 250°C. The purpose of studying these three specific temperatures was to examine adsorption levels above, at, and below the critical temperature of pyridine (347°C).

The ammonia adsorption experiments were completed by mixing appropriate ammonia and helium gas ratios which corresponded to the pyridine concentrations. Ammonia flow rates ranged from 1.5 cm³/min to 14.0 cm³/min. However, the adsorption temperatures were identical to those used during pyridine adsorption.

CHAPTER IV

EXPERIMENTAL RESULTS

The results which are contained within this chapter consist of equilibrium and transient adsorption data, catalyst reduction data, and poison reversibility data. Ammonia demonstrated interesting behavior in that it reduced the catalyst rather than demonstrating only adsorption characteristics. Hydrogen adsorption was also investigated and it was found that hydrogen also reduced the catalyst surface. This result was expected for hydrogen, but not for ammonia. Finally, in order to investigate whether or not the poison was adsorbed reversibly or irreversibly and to substantiate the claim that coke may be forming on the catalyst surface, a reversibility experiment was completed.

The equilibrium adsorption data for pyridine are listed in Table III. The corresponding adsorption isotherms for pyridine are shown in Figure 2. The pyridine partial pressure range is 284 N/m^2 to 2130 N/m^2 . As adsorption temperature decreased the equilibrium adsorption weight increased. The 350°C and 250°C data appear to reach an asymptote where adsorbed weight is not a function of partial pressure. This behavior is characteristic of Type I adsorption isotherms (idealized Langmuir adsorption). However, the data at 450°C do demonstrate a dependence on partial pressure. One point which should be made about the adsorption data is that as pyridine concentration increases one might expect buoyancy to have an effect on the equilibrium results.

TABLE III
PYRIDINE EQUILIBRIUM ADSORPTION DATA

Run	Cat. Wt. (mg)	Ads. Temp. (°C)	P_{py} (N/m ²)	Ads. Wt. (mg/g cat.)	θ_p^*
15	11.4119	400	1110	9.814	0.078
		350		12.269	0.098
		250		20.154	0.161
17	13.1218	450	1620	6.630	0.053
19	8.5859	450	608	2.574	0.021
21	12.1720	450	608	1.360	0.011
		350		10.598	0.085
		250		20.703	0.165
22	15.9919	450	1220	6.979	0.056
		350		11.131	0.089
		250		13.263	0.106
23	11.1750	450	2130	8.217	0.066
		350		12.989	0.104
		250		19.596	0.157
24	12.5560	450	1820	4.380	0.035
		350		10.067	0.080
		250		17.044	0.136

TABLE III (Continued)

Run	Cat. Wt. (mg)	Ads. Temp. (°C)	P_{py} (N/m ²)	Ads. Wt. (mg/g cat.)	θ_p^*
25	10.9435	450	284	1.873	0.015
		350		11.742	0.094
		250		19.336	0.155

* Fractional surface coverage based on 208 m² surface area/g cat. and pyridine molecule surface area is 2.18x10⁻¹⁹ m²/molecule. Molecular size was calculated from Lennard-Jones collision diameter parameter for benzene (Entz, 1984).

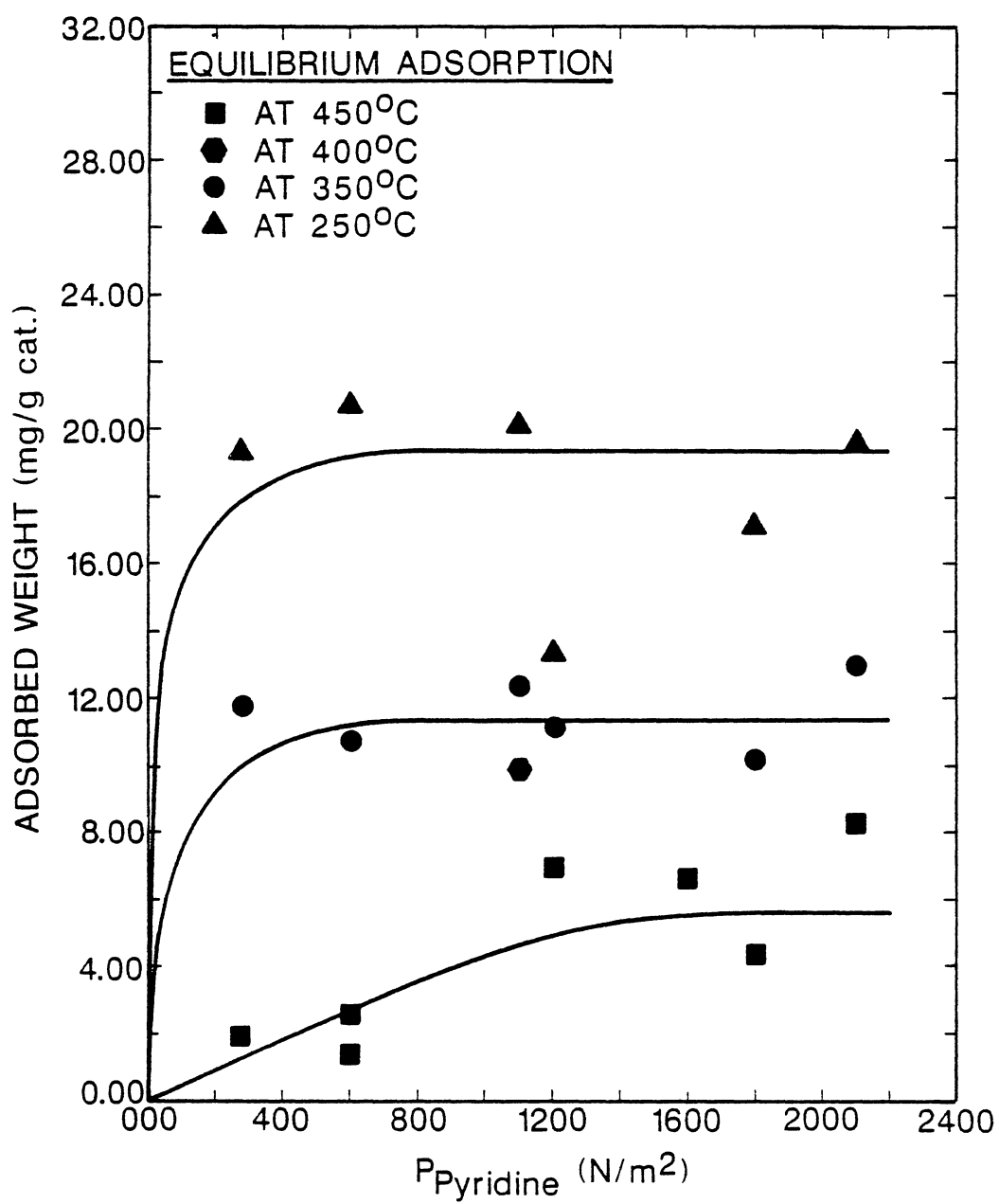


Figure 2. Equilibrium Adsorption Isotherms for Pyridine

However, buoyancy calculations were completed (see Appendix A) and buoyancy was found to have a negligible effect on the measured weight gain in the partial pressure range used.

The transient adsorption data for pyridine poisoning of the catalyst are shown in Table IV. The 350°C and 250°C transient data have not been reported. The reason for this is because they can not be compared to the 450°C data. The 450°C data were collected while adsorbing pyridine on a fresh catalyst at a constant temperature. While changing the system temperature to 350°C and 250°C pyridine was constantly exposed to the same catalyst. Thus, the transient data for these two temperatures occurred while the temperature was not constant. However, the equilibrium values are not believed to have been affected.

The data from Table IV have been plotted and appear in Figure 3. Some of the experimental data, although producing consistent equilibrium values, demonstrated unusual transient behavior. As such, some of the data which appear in Figure 2 do not have a corresponding transient representation. The data in Figure 3 do not exhibit a direct relationship between partial pressure and transient behavior. For example, Run 24 data ($P_{py} = 1812 \text{ N/m}^2$) do not lie between Run 23 ($P_{py} = 2130 \text{ N/m}^2$) and Run 22 ($P_{py} = 1220 \text{ N/m}^2$) data. However, Run 15, which was completed at 400°C, definitely shows more rapid adsorption than the data which was taken at 450°C.

One of the results indicated by Entz (13) was that hydrogen adsorbed on the oxidic state of a NiMo/Al₂O₃ catalyst. One expects the hydrogen to reduce the catalyst by reacting with the metal oxides to form water (H₂O). Table V and Figure 4 demonstrate experimentation to

TABLE IV
TRANSIENT ADSORPTION DATA

Run	Temp. (°C)	Cat. Wt. (mg)	t (min)	Ads. Wt. (mg/g cat.)	P_{py} (N/m ²)
15	400	11.4119	0	0.000	1110
			24	0.622	
			48	2.112	
			72	4.119	
			120	5.135	
			180	6.537	
			240	7.282	
			300	8.027	
			360	8.465	
			480	9.078	
			600	9.578	
			720	9.841	
			900	9.814	
			1140	9.814	
17	450	13.1218	0	0.000	1620
			24	0.625	
			48	1.235	
			72	1.806	
			120	2.774	
			180	3.102	
			300	3.788	
			420	4.588	

TABLE IV (Continued)

Run	Temp. (°C)	Cat. Wt. (mg)	t (min)	Ads. Wt. (mg/g cat.)	P_{py} (N/m ²)
17 (continued)			540	4.908	
			780	5.647	
			1020	6.112	
			1260	6.455	
			1380	6.554	
			1680	6.630	
			1740	6.630	
22	450	15.9919	0	0.000	1220
			24	1.132	
			48	1.695	
			72	2.689	
			108	3.264	
			408 (168)*	3.977	
			588 (348)	5.021	
			768 (528)	5.665	
			948 (708)	6.353	
			1128 (888)	6.791	
			1248 (1008)	7.022	
			1488 (1248)	6.979	
			1608 (1368)	6.979	

TABLE IV (Continued)

Run	Temp. (°C)	Cat. Wt. (mg)	t (min)	Ads. Wt. (mg/g cat.)	P _{py} (N/m ²)
23	450	11.1350	0	0.000	2130
			24	1.706	
			48	3.368	
			84	4.311	
			144	4.60	
			264	5.191	
			444	5.972	
			564	6.29	
			684	7.095	
			864	7.723	
			1044	8.181	
			1224	8.217	
24	450	12.5560	0	0.000	1820
			24	2.071	
			48	3.026	
			84	3.106	
			144	3.146	
			204	3.496	
			264	3.903	
			384	4.165	
			444	4.261	
			624	4.420	
			744	4.380	

TABLE IV (Continued)

Run	Temp. (°C)	Cat. Wt. (mg)	t (min)	Ads. Wt. (mg/g cat.)	P _{py} (N/m ²)
25	450	10.9435	0	0.000	284
			12	0.676	
			24	1.115	
			36	1.416	
			48	1.645	
			72	1.736	
			132	1.800	
			192	1.855	
			252	1.873	

* There was a system leak and pyridine desorbed from catalyst for four hours. Values which appear in parentheses represent a four hour difference from the actual time.

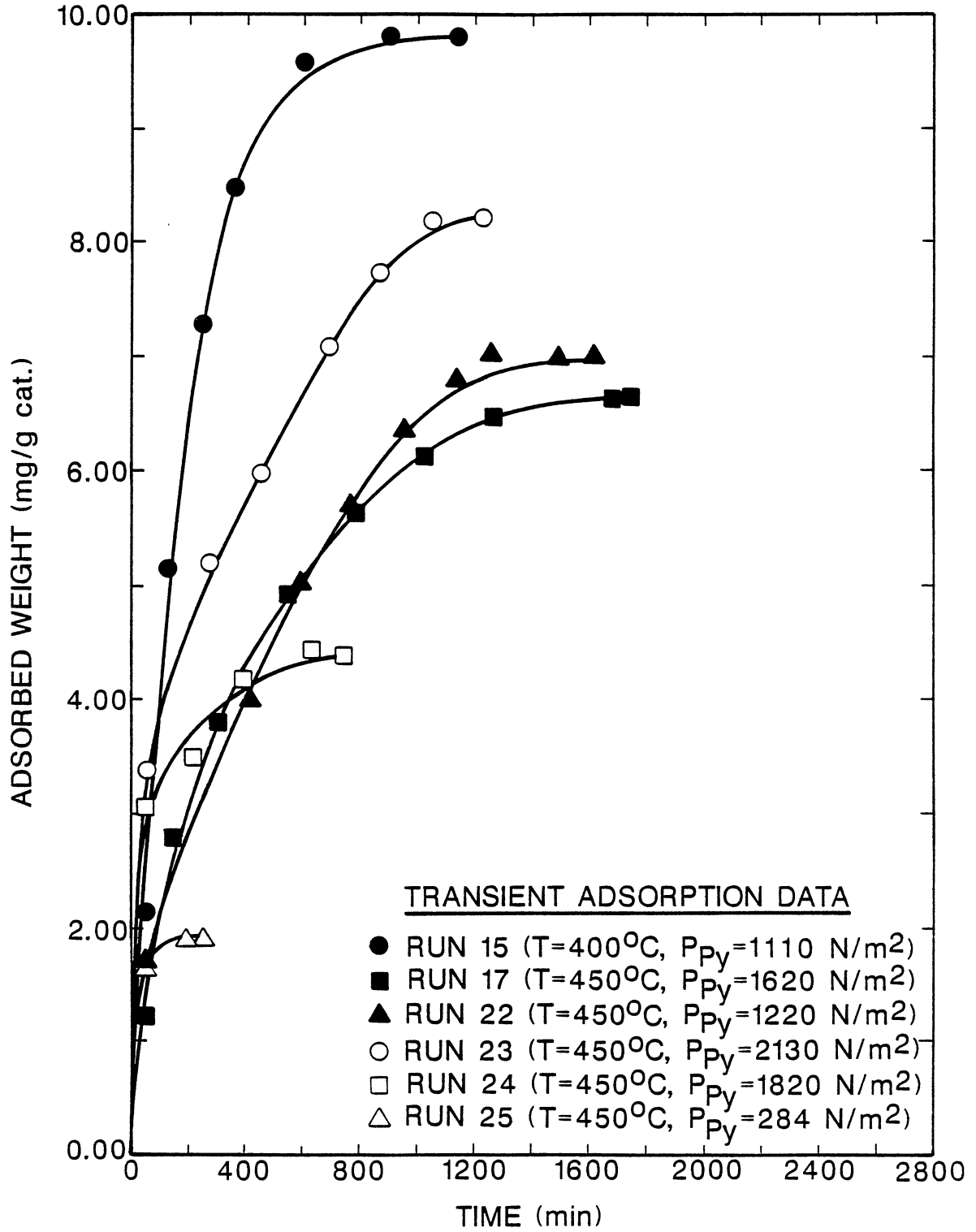


Figure 3. Transient Pyridine Adsorption Behavior

TABLE V
CATALYST REDUCTION DATA

Run	Type of Reduction	Oxygen Available for Reduction			Wt. Loss
		Total	NiO	MoO ₃	
27	H ₂	0.90 mg	0.09 mg	0.81 mg	0.27 mg
26	NH ₃	0.94 mg	0.09 mg	0.85 mg	0.10 mg
28	NH ₃	0.94 mg	0.09 mg	0.85 mg	0.07 mg

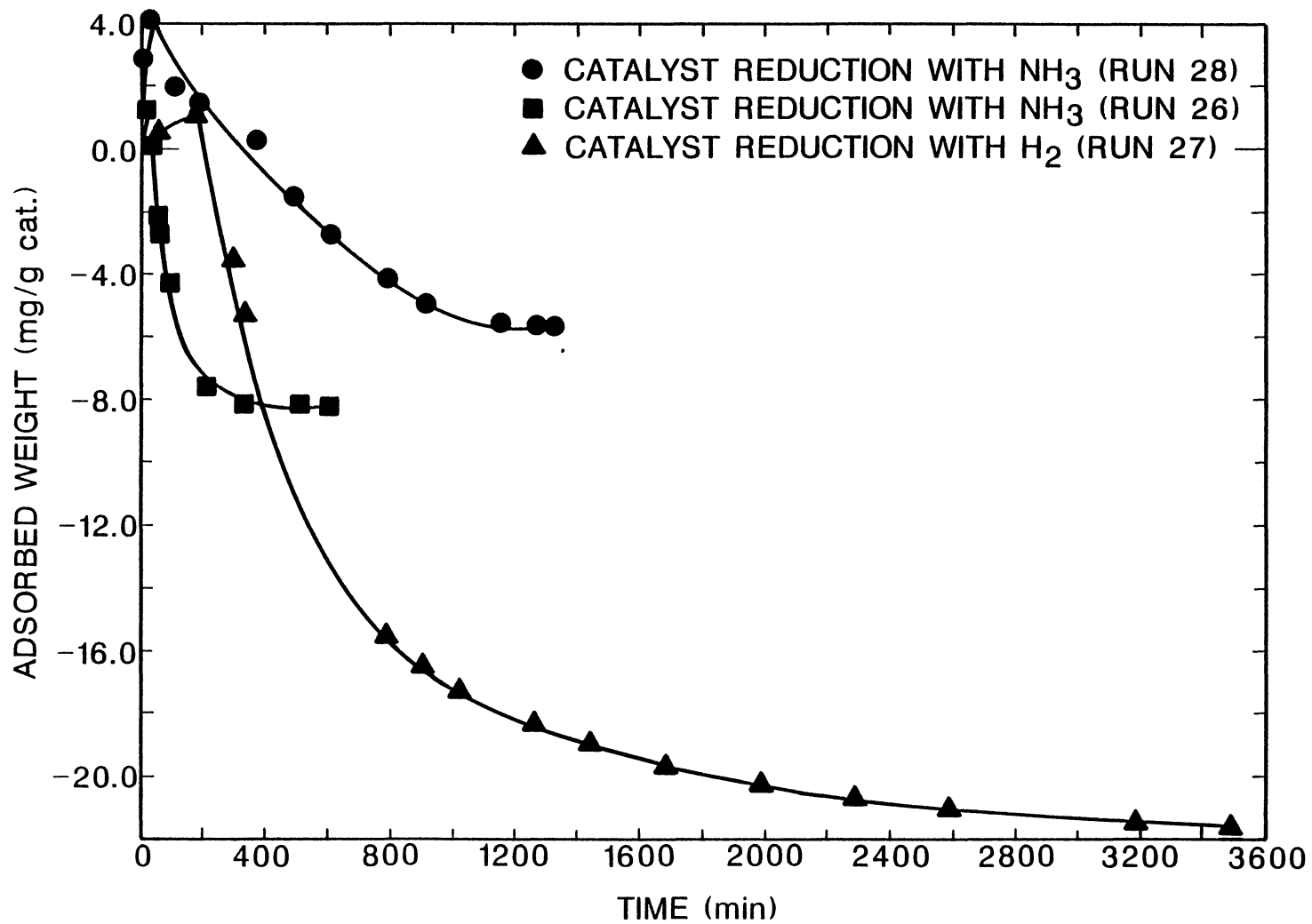


Figure 4. Catalyst Reduction Behavior Due to Hydrogen and Ammonia Adsorption

investigate whether or not the Shell 324 catalyst would reduce in the presence of hydrogen. Figure 4 indicates the catalyst did reduce in the presence of hydrogen which conflicts with Entz's results.

Ammonia adsorption was also attempted and an interesting result occurred. Upon exposure to ammonia, the oxidic catalyst underwent reduction. The reduction data due to ammonia are also demonstrated in Table V and Figure 4. Appendix C contains the calculations made to determine what percentage of oxygen was available as NiO and MoO₃ and how the amount of weight loss compared to these values. The comparisons are shown in Table V.

Table VI and Figure 5 contain data from a reversibility experiment. This experiment was used to support the claim that coke had formed on the catalyst surface at 450°C. As can be seen in Figure 5, a 33% irreversibility occurred during this experiment. The poison desorption between 5 and 15 hours can be attributed to a system leak, which was subsequently corrected. The dashed line indicates an approximation of the adsorption curve if the system leak had not occurred.

TABLE VI
PYRIDINE ADSORPTION/DESORPTION DATA

Run	Temp. (°C)	Cat. Wt. (mg)	t (min)	Ads. Wt. (mg/g cat.)	P _{py} (N/m ²)
14	450	13.1205	0	0.00	1620
			1	7.09	
			5	8.80	
			8	7.87	
			13	5.64	
			15	8.41	
			20	11.05	
			25	11.60	
			30	13.08	
			35	13.38	
			38	13.38	
			40	12.13	
			45	9.68	
			50	7.74	
			55	6.71	
			60	5.64	
65	4.99				
70	4.63				
75	4.37				

Initial catalyst weight - 13.1205 mg
 Catalyst weight after adsorption - 13.2960 mg
 Catalyst weight after desorption - 13.1778 mg*

* This demonstrates a 33% irreversibility which is attributed to coke formation on the catalyst surface.

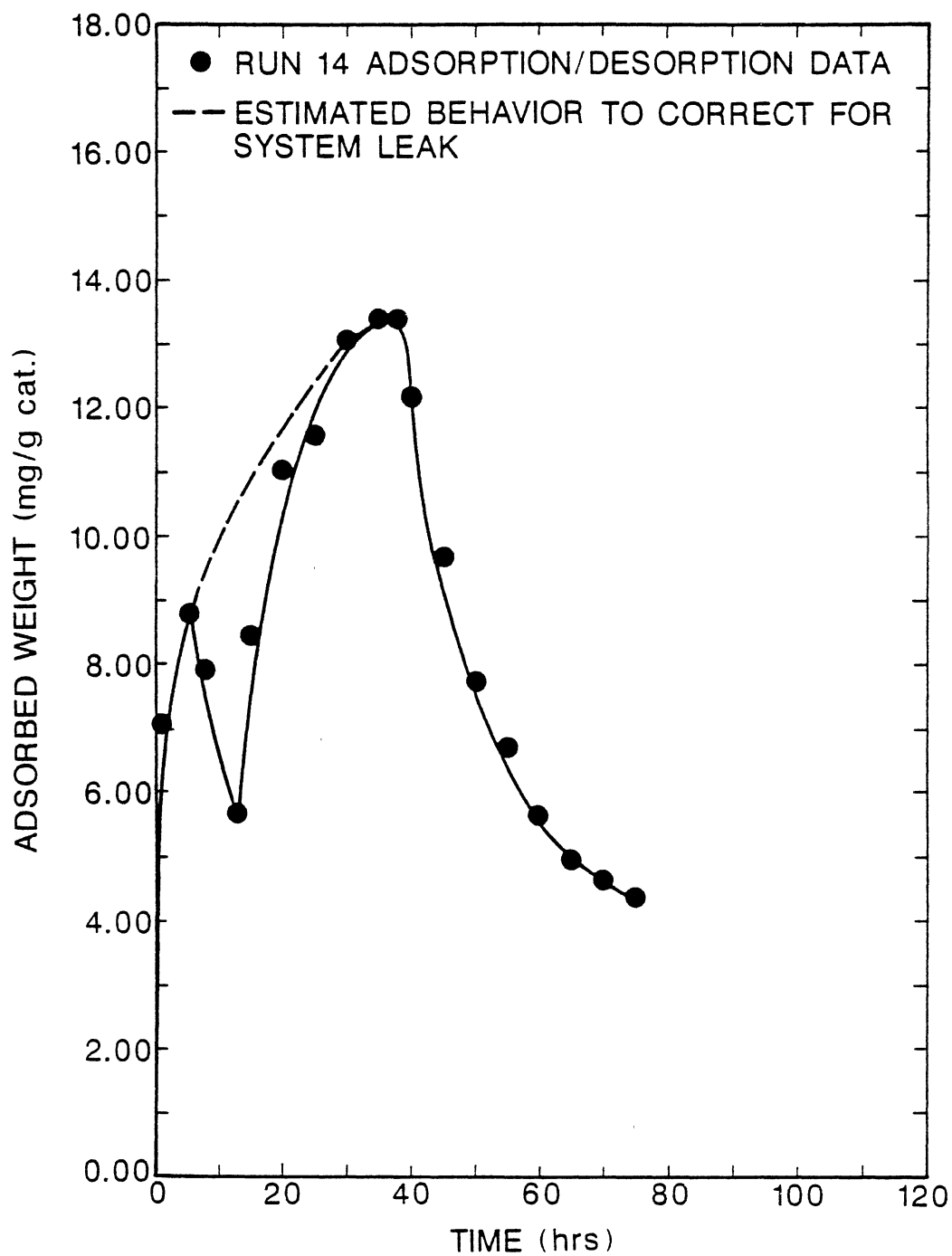


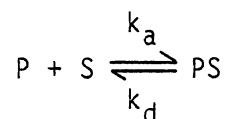
Figure 5. Pyridine Adsorption Reversibility Behavior

CHAPTER V

DISCUSSION

The equilibrium adsorption data in Figure 2 show that as adsorption temperature decreases the amount of adsorbed poison increases. Furthermore, as the adsorption temperature decreases below the critical temperature of pyridine (347°C) one might expect multilayer adsorption to occur on the catalyst surface. However, Table III shows that the maximum fractional surface coverage by pyridine at 250°C is only about 16% of the total catalyst surface area. Multilayer coverage may be occurring at low temperatures but not over the entire catalyst surface. It may be that the number of strong active sites (strong acidic behavior) only cover about 16% of the catalyst surface.

One parameter which is useful to calculate from equilibrium reaction data is the equilibrium constant for the reaction and the heat of reaction (adsorption). In order to determine the equilibrium constant one needs to know the reaction rate equation. One can represent the poisoning of the active sites by:



P denotes the reactant poison, S denotes a catalyst active site, and PS represents adsorbed poison on a catalyst site. The rate of adsorption on the catalyst site is given by:

$$\frac{dC_{PS}}{dt} = k_a P_P C_S - k_d C_{PS} \quad (1)$$

where,

C_{PS} \equiv quantity of active sites occupied by poison, P, mass/g cat.

C_S \equiv quantity of unoccupied catalyst active sites at any time,
mass/g cat.

P_P \equiv partial pressure of poison, P, N/m².

k_a \equiv adsorption rate constant, m²/N min⁻¹.

k_d \equiv desorption rate constant, min⁻¹.

At equilibrium the rate of poison adsorption is zero ($\frac{dC_{PS}}{dt} = 0$), and Equation 1 becomes:

$$k_a P_P C_S = k_d (C_{PS})_{eq} \quad (2)$$

A balance on the active sites which are found on a catalyst surface gives:

$$C_{S_0} = C_S + C_{PS}$$

where,

C_{S_0} \equiv quantity of fresh catalyst active sites, mass/g cat.

Substitution of this active site balance into Equation 2 gives:

$$k_a P_P [C_{S_0} - (C_{PS})_{eq}] = k_d (C_{PS})_{eq}$$

$$(C_{PS})_{eq} = \frac{k_a P_p C_{S_0}}{k_a P_p + k_d}$$

Now introduce the equilibrium constant:

$$K = \frac{k_a}{k_d}$$

$$(C_{PS})_{eq} = \frac{KP_p C_{S_0}}{KP_p + 1} \quad (3)$$

Equation 3 suggests the equilibrium level of poison adsorption has a partial pressure dependence. However, Figure 2 does not show this partial pressure dependence for the 350°C and 250°C data. Thus, the 350°C and 250°C data were taken in a range where $KP_p \gg 1$ (K is thus indeterminable) and this eliminated the partial pressure dependence of the equilibrium adsorption weight term:

$$(C_{PS})_{eq} = C_{S_0}$$

The 450°C data, do however, indicate a partial pressure dependence and will allow an equilibrium constant to be evaluated from Equation 3. The equilibrium data at 450°C indicate an equilibrium constant of $K = 37.0$. However, Smith (27) suggests that the determination of equilibrium constants from Langmuir theory (which is what Equation 3 is describing) rarely agrees with the values of the constants determined from the reaction rate data. This deviation may be attributed to interaction effects between components, surface heterogeneity, and other inadequacies of the Langmuir theory.

An attempt was made to relate equilibrium adsorption weight to temperature. One possible relation would be to use the Van't Hoff equation which allows the heat of adsorption to be calculated from the dependence of the equilibrium constant on temperature. However, as already discussed, one can conclude from Equation 3 that the experimental data lie in a region where $KP_p \gg 1$. This has the effect that K is indeterminable from the equilibrium data. However, a linear plot of equilibrium adsorption weight versus absolute temperature is justified and this appears in Figure 6. Although there are only three data points, there seems to be a linear dependence of equilibrium adsorption weight on temperature. Before any firm conclusions should be drawn, more data needs to be taken in both the $KP_p \gg 1$ and $KP_p \ll 1$ regions.

One might speculate that since the amount of adsorption increases with decreasing temperature, the number of active sites, C_{S_0} , is also a function of temperature. As the system temperature is changed the catalyst may undergo a physical change (e.g. thermally induced crack propagation). This change may create more surface area and thus expose more active sites. However, the range of temperatures during the current experimentation (450°C - 250°C) does not seem severe enough to cause any physical catalyst changes. The behavior is probably better explained by a condensation effect where more poison condenses on top of previous poison layers as the temperature decreases.

The transient adsorption data are shown in Figure 3. Note that Runs 19 and 21, which appear as equilibrium data in Figure 2, do not appear on the transient data figure (Figure 3). The reason for this is that excessive leak problems produced poor transient data but reasonably

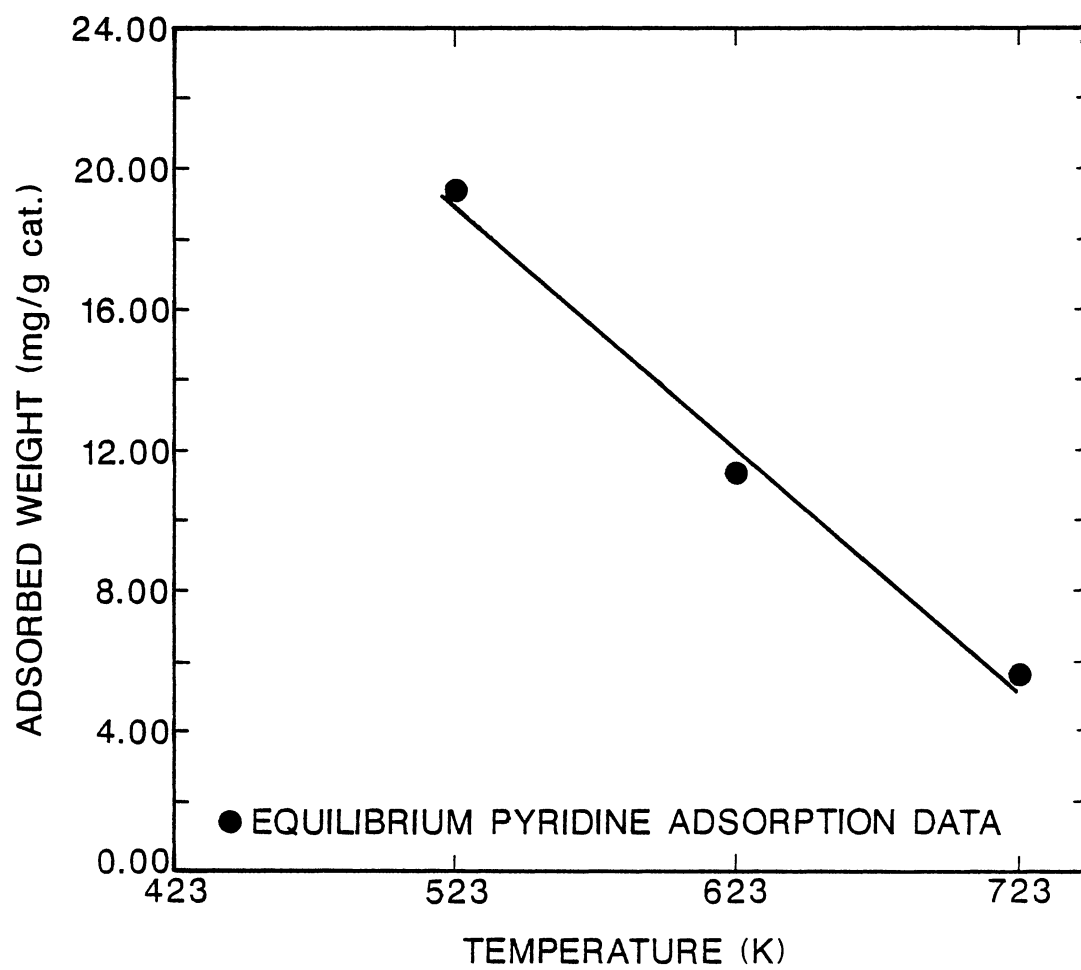


Figure 6. Equilibrium Adsorption Weight Dependence on Temperature

reproducible equilibrium data. There does not seem to be a direct relation between the transient adsorption data and partial pressure. One may expect the rate of adsorption to be greater with a higher partial pressure, but this is not the case. Run 22 ($P_{py} = 1220 \text{ N/m}^2$) transient data lie between Run 23 ($P_{py} = 2130 \text{ N/m}^2$) and Run 24 ($P_{py} = 1820 \text{ N/m}^2$) data. The only definite relationship which can be seen is that as temperature is decreased (Run 15 - 400°C) the rate of adsorption and equilibrium adsorption values both increase.

One of the advantages of using a thermal gravimetric analyzer is that it allows constant monitoring of the adsorption process. As such, a fairly large amount of transient adsorption data has been obtained. A common method to analyze these data is to try and model the poisoning mechanism. The first step in attempting to model the poisoning mechanism is to look at the kinetics of the poisoning reaction. The rate of adsorption of poison can be described by Equation 1.

Recall the active site balance was given by:

$$C_{S_0} = C_S + C_{PS}$$

Substitution of this site balance into Equation 1 gives:

$$\begin{aligned} \frac{dC_{PS}}{dt} &= k_a P_P (C_{S_0} - C_{PS}) - k_d C_{PS} \\ \frac{dC_{PS}}{dt} &= k_a P_P C_{S_0} - (k_a P_P + k_d) C_{PS} \end{aligned} \quad (4)$$

Before integrating this equation, define a variable, α_1 , as follows:

$$\alpha_1 = k_a P_p C_{S_0} - (k_a P_p + k_d) C_{PS}$$

Differentiation of α_1 with respect to time gives:

$$\frac{d\alpha_1}{dt} = - (k_a P_p + k_d) \frac{dC_{PS}}{dt}$$

Substitution into Equation 4 gives:

$$\frac{d\alpha_1}{dt} = - (k_a P_p + k_d) \alpha_1$$

Now integrate this equation to give:

$$\ln \alpha_1 = -(k_a P_p + k_d)t + C$$

Where C is the constant of integration. The initial condition for this integral is:

$$\text{at } t = 0, C_{PS} = 0 \quad (\alpha_1 = \alpha_0)$$

$$\ln \alpha_1 = - (k_a P_p + k_d)t + \ln \alpha_0$$

$$\ln \left[\frac{\alpha_1}{\alpha_0} \right] = - \beta t$$

where,

$$\beta = (k_a P_p + k_d)$$

Now replace α_1 with the appropriate terms:

$$\ln \left[\frac{k_a P_p C_{S_0} - (k_a P_p + k_d) C_{PS}}{k_a P_p C_{S_0}} \right] = -\beta t$$

At equilibrium the rate of poison adsorption is zero, therefore

$$(C_{PS})_{eq} = \frac{k_a P_p C_{S_0}}{k_a P_p + k_d}$$

Dividing all the terms inside the log term by $(k_a P_p + k_d)$ gives:

$$\ln \left[\frac{(C_{PS})_{eq} - C_{PS}}{(C_{PS})_{eq}} \right] = -\beta t \quad (5)$$

The model of Equation 5 represents the reversible poisoning of a catalyst. A plot of $[(C_{PS})_{eq} - C_{PS}]/(C_{PS})_{eq}$ versus time on semi-logarithmic paper should produce a straight line with slope of $-\beta$. This plot is demonstrated with the data from Run 17 in Figure 7.

The reversible poisoning model is a single exponential model and the semi-logarithmic plot in Figure 7 should demonstrate linear behavior if the model describes the experimental data. This expected behavior is indicated by the dashed line in Figure 7. However, the experimental data definitely demonstrate a deviation from this line in the 100-500 minute time period. Furthermore, the behavior of the data suggest that two exponential models may produce a better data fit. These regions are indicated by the two solid lines with the different slopes in Figure 7. The solid line with a smaller slope in Figure 7 has been extrapolated to time-zero in order to determine the y-intercept.

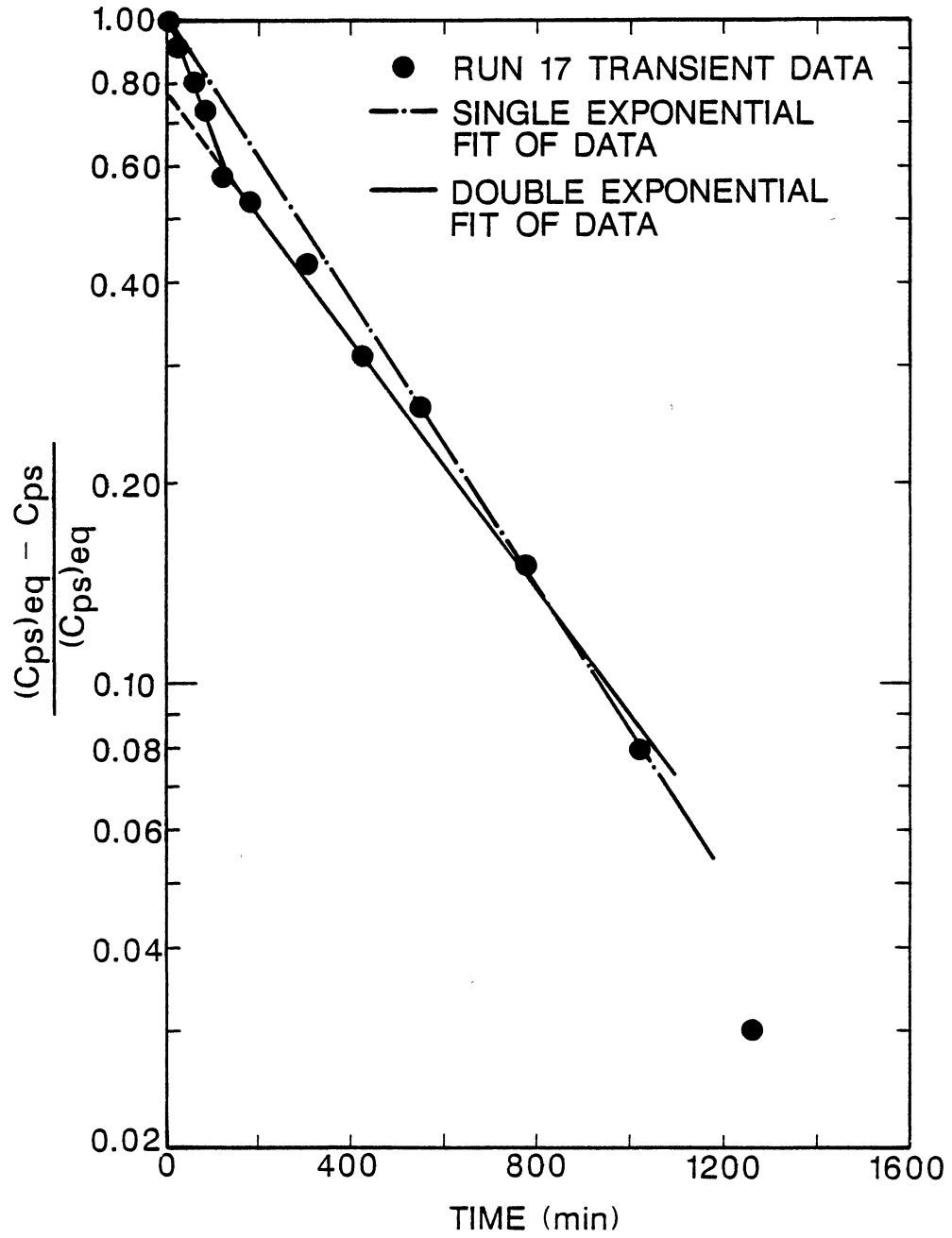


Figure 7. Reversible Poisoning Model Log Plot of Run 17 Transient Data

Before attempting any further modeling, the reversible poisoning model was used to predict the transient adsorption data of Run 17. Figure 8 demonstrates this prediction and the comparison to experimental adsorption data. The slope of the model, $-\beta$, was calculated based on the dashed line in Figure 7. There are several observations which need to be stated about the model fit of Figure 7 and prediction of Figure 8. First, the data in Figure 8 tend to lie slightly above most of the predicted line. This suggests that there may be something contributing to the catalyst weight in addition to reversible poisoning. One possibility may be that coke formation is occurring simultaneously with poison adsorption. Coke formation is substantiated by the following observations: 1) a reversibility experiment indicated that 33% of what was adsorbed on the catalyst surface was irreversibly held on the surface, and 2) the catalyst changed from a light green-yellow color at the beginning of the 450°C adsorption experiments to a grey color at the end of the experiments.

Pore diffusion limitations on adsorption are not believed to be dominant because one would expect this type of behavior to produce a reversible poisoning prediction higher than the experimental data. Furthermore, a simplistic adsorption model based on a progressive shell model for diffusion (developed in Appendix B) indicates a poor fit of the experimental data.

Another important observation is that a steady-state adsorption level is achieved as indicated by the equilibrium values in Figure 2. This suggests that sometime during the adsorption run the coke formation reaches a steady-state value. In the absence of hydrogen, coke formation is probably very rapid and may reach a very rapid steady-

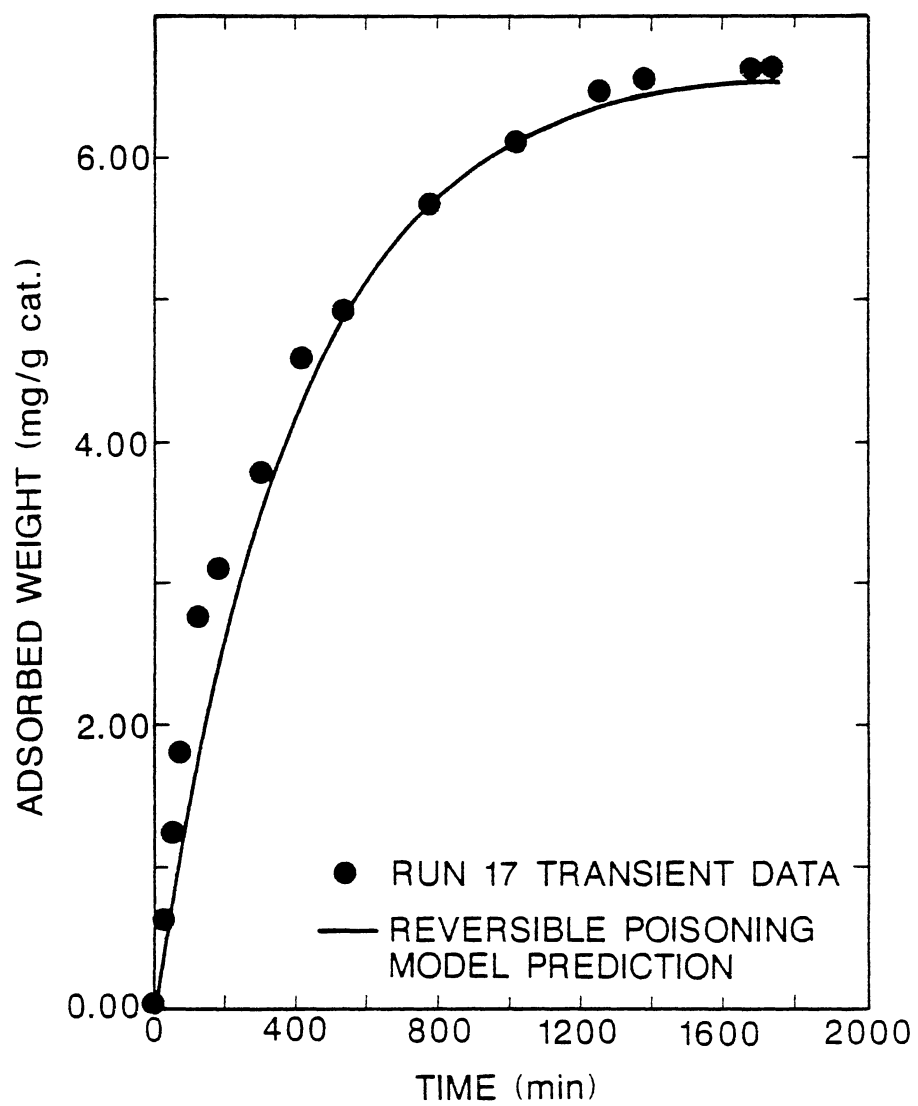


Figure 8. Run 17 Transient Adsorption Data Prediction from Reversible Poisoning Model

state. The time required for a steady-state coke level is unknown but the data in Figure 7 indicate it may be somewhere in the first 100 minutes. Furthermore, the behavior of the data in Figure 7 suggest that simultaneous coking and poisoning is occurring up to the point where the solid line breaks slope. At the break in slope the coke level may have reached a steady-state and the lower solid line is indicating only reversible poisoning. The reason for extending the reversible poisoning line (solid line with smaller slope) to the y-axis is to approximate the coke content of the catalyst. The plot in Figure 7 suggests the coke content is approximately 25% and this is quite close to the value obtained from reversibility experiments (33%). One may find that the sites which induce coke formation are those sites which surround the dehydrogenation metal sites or those which are highly acidic. In any case, coke formation probably deactivates these sites rapidly and thus attains a rapid steady-state level.

Assuming that the simultaneous coke formation and reversible poisoning mechanism explains the data, two models must now be formulated. One model will account for the initial simultaneous coke formation and poisoning. The other model will account for reversible poisoning after a steady-state coke level has been attained. The latter model will be developed first.

The rate of poison accumulation is given by Equation 1, however, the active site balance must now include the sites which are covered by coke (which is a constant because the rate of coke deposition is assumed to be zero in this model).

$$C_{S_0} = C_S + C_{PS} + C_C$$

where $C_C \equiv$ quantity of active sites occupied by coke, C, mass/g cat.

Substitution of this balance into Equation 1 gives:

$$\frac{dC_{PS}}{dt} = k_a P_P (C_{S_0} - C_{PS} - C_C) - k_d C_{PS} \quad (6)$$

The electrobalance which was used to obtain the transient adsorption data measured total weight changes. This total weight includes both poison adsorption and coke formation. Thus, define a variable, W, which accounts for these two components:

$$W = C_{PS} + C_C$$

Differentiating with respect to time gives:

$$\frac{dW}{dt} = \frac{dC_{PS}}{dt} + \frac{dC_C}{dt}$$

This model is being developed for the period when rate of coke formation is zero ($\frac{dC_C}{dt} = 0$), thus

$$\frac{dW}{dt} = \frac{dC_{PS}}{dt}$$

Substitution of W instead of C_{PS} and C_C in Equation 6 gives:

$$\frac{dW}{dt} = k_a P_P (C_{S_0} - W) - k_d (W - C_C)$$

Rearrangement yields:

$$\frac{dW}{dt} = (k_a P_P C_{S_0} + k_d C_C) - (k_a P_P + k_d)W \quad (7)$$

Now define a variable, α_2 , to simplify integration:

$$\alpha_2 = (k_a P_P C_{S_0} + k_d C_C) - (k_a P_P + k_d)W$$

$$\frac{d\alpha_2}{dt} = - (k_a P_P + k_d) \frac{dW}{dt}$$

Substitution into Equation 7 gives:

$$\frac{d\alpha_2}{dt} = -(k_a P_P + k_d)\alpha_2$$

Integration yields:

$$\ln \alpha_2 = -(k_a P_P + k_d)t + K$$

where K is the integration constant which can be found by using the following boundary condition:

$$\text{at } t = t_C, W = W_C (\alpha_2 = \alpha_C)$$

where,

$t_C \equiv$ time required for steady-state coke level to be achieved, min.

$W_C \equiv$ amount of poison and coke deposited on catalyst at time t_C ,
mg/g cat.

Solving for the integration constant yields:

$$K = \ln \alpha_C + (k_a P_p + k_d) t_C$$

Substitution into the integrated equation gives:

$$\ln \left[\frac{\alpha_2}{\alpha_C} \right] = (k_a P_p + k_d) (t_C - t)$$

Now replace α_2 with appropriate terms to give:

$$\ln \left[\frac{(k_a P_p C_{S_0} + k_d C_C) - (k_a P_p + k_d) W}{(k_a P_p C_{S_0} + k_d C_C) - (k_a P_p + k_d) W_C} \right] = - (k_a P_p + k_d) (t - t_C)$$

At equilibrium, $\frac{dW}{dt} = 0$, and Equation 7 becomes:

$$k_a P_p C_{S_0} + k_d C_C = (k_a P_p + k_d) W_{eq}$$

$$W_{eq} = \frac{k_a P_p C_{S_0} + k_d C_C}{k_a P_p + k_d}$$

Dividing all components of the log term by $(k_a P_p + k_d)$ gives

$$\ln \left[\frac{W_{eq} - W}{W_{eq} - W_C} \right] = - \beta_2 (t - t_C) \quad (8)$$

where,

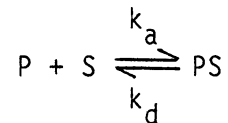
$$\beta_2 = (k_a P_p + k_d)$$

This model should now account for reversible poison adsorption on a catalyst surface which has a constant coke layer already adsorbed. In

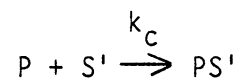
order to find t_C and W_C one needs to first use the reversible poisoning model of Equation 5 and plot $\ln[(C_{PS})_{eq} - C_{PS}]/(C_{PS})_{eq}$ versus time. W_C can be obtained at the break in slope which occurs at t_C .

Figure 9 demonstrates this reversible poisoning model plot, for Runs 17 and 23, which allows t_C and W_C to be obtained. Values for t_C and W_C for each run are given in Table VII.

Now the model which describes the initial simultaneous coke formation and reversible poisoning of a catalyst will be developed. In order to represent the poisoning mechanism assume that poison is adsorbed on two types of sites. The first site, S, results in reversible adsorption of the poison and can be represented by:



The second site, S', results in irreversible adsorption of the poison which then forms coke. The coking mechanism can be described by:



where,

$k_c \equiv$ coke formation rate constant, $m^2/N \text{ min}^{-1}$.

It has also been determined that the TGA monitors total weight changes (due to coking and poisoning) and that:

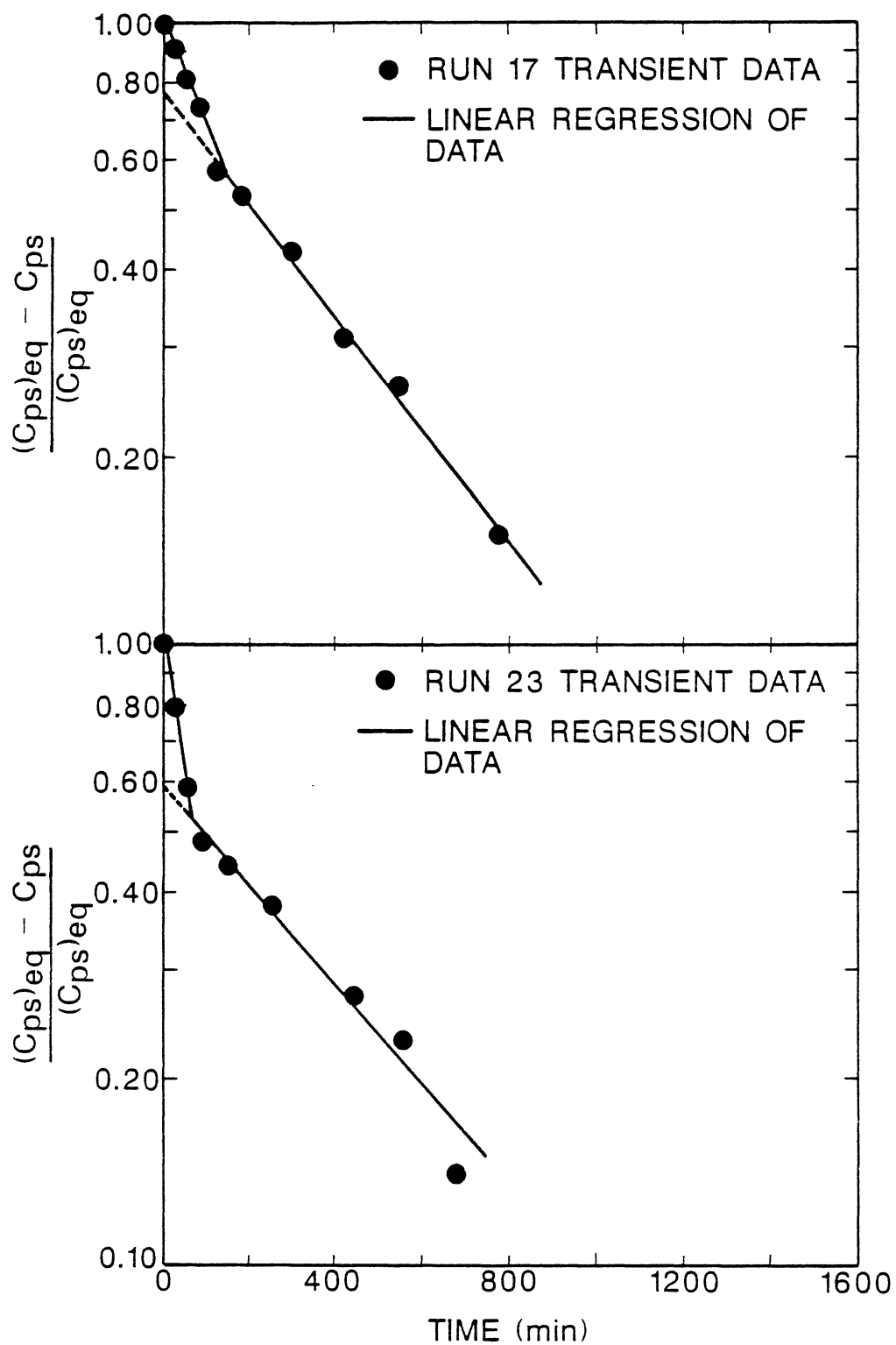


Figure 9. Reversible Poisoning Model Log Plot of Run 17 and 23 Transient Data

TABLE VII
CATALYST COKE CONTENT DATA

Run	t_C (min)	W_C (mg/g cat.)	$(C_{PS})_{eq}$ (mg/g cat.)
15	-	*	9.814
17	150	2.849	6.630
22	133	3.800	6.979
23	76	3.942	8.217
24	60	2.847	4.380
25	-	*	1.873

* Runs 15 and 25 did not demonstrate coking behavior.

$$W = C_{PS} + C_{PS'}$$

and,

$$\frac{dW}{dt} = \frac{dC_{PS}}{dt} + \frac{dC_{PS'}}{dt} \quad (9)$$

The rate of poison adsorption is given by:

$$\frac{dC_{PS}}{dt} = k_a P_P C_S - k_d C_{PS}$$

The rate of coke formation is given by:

$$\frac{dC_{PS'}}{dt} = k_c P_P C_{S'}$$

Substitution of these expressions into Equation 9 gives:

$$\frac{dW}{dt} = k_a P_P C_S - k_d C_{PS} + k_c P_P C_{S'} \quad (10)$$

The active site balance must now include, in addition to sites covered by coke, unoccupied active sites available for coking:

$$C_{S_0} = C_S + C_{PS} + C_{S'} + C_{PS'}$$

$$C_{S_0} = C_S + C_{S'} + W$$

Substitution of the active site balance in Equation 10 gives:

$$\frac{dW}{dt} = k_a P_P (C_{S_0} - C_{S'} - W) - k_d (W - C_{PS'}) + k_c P_P (C_{S_0} - C_S - W)$$

Rearrangement yields:

$$\frac{dW}{dt} = [k_a P_P (C_{S_0} - C_{S'}) + k_c P_P (C_{S_0} - C_S) + k_d C_{PS'}] - (k_a P_P + k_d + k_c P_P)W \quad (11)$$

In order to simplify integration, define a variable, α_3 , as follows:

$$\alpha_3 = k_a P_P (C_{S_0} - C_{S'}) + k_c P_P (C_{S_0} - C_S) + k_d C_{PS'} - (k_a P_P + k_d + k_c P_P)W$$

Differentiation with respect to time yields:

$$\frac{d\alpha_3}{dt} = - (k_a P_P + k_d + k_c P_P) \frac{dW}{dt}$$

Substitution into Equation 11 gives:

$$\frac{d\alpha_3}{dt} = - (k_a P_P + k_d + k_c P_P) \alpha_3$$

Integration yields:

$$\ln \alpha_3 = - \beta_1 t + C$$

where,

$$\beta_1 = (k_a P_P + k_d + k_c P_P)$$

and the initial condition is:

$$\text{at } t = 0, W = 0 (\alpha_3 = \alpha')$$

$$\ln \left[\frac{\alpha_3}{\alpha'} \right] = - \beta_1 t$$

Substitution of α_3 gives

$$\ln \left[\frac{k_a P_P (C_{S_0} - C_{S'}) + k_c P_P (C_{S_0} - C_S) + k_d C_{PS'}}{k_a P_P (C_{S_0} - C_{S'}) + k_c P_P (C_{S_0} - C_S) + k_d C_{PS'}} - \frac{(k_a P_P + k_d + k_c P_P) W}{k_a P_P (C_{S_0} - C_{S'}) + k_c P_P (C_{S_0} - C_S) + k_d C_{PS'}}} \right]$$

$$= - \beta_1 t$$

At equilibrium, $\frac{dW}{dt} = 0$, and Equation 11 becomes:

$$W_{eq} = \frac{k_a P_P (C_{S_0} - C_{S'}) + k_c P_P (C_{S_0} - C_S) + k_d C_{PS'}}{k_a P_P + k_c P_P + k_d}$$

Dividing all components of the log term by $(k_a P_P + k_c P_P + k_d)$ gives:

$$\ln \left[\frac{W_{eq} - W}{W_{eq}} \right] = - \beta_1 t \quad (12)$$

These two models (Equations 8 and 12) can now be used to describe the two regimes of poisoning. The first regime ($0 < t < t_C$) being when simultaneous coking and reversible poison adsorption are occurring, and the second regime being when a constant level of coke has formed and only reversible poison adsorption is occurring ($t > t_C$).

A linear regression routine was used to obtain the β_1 and β_2 parameters for all sets of transient adsorption data. The results of this analysis are listed in Table VIII.

Figures 10-13 demonstrate the fit of the two exponential models with the experimental data. There was a system leak during Run 22 and the model fit should be compared to the data represented by the open circles rather than the solid circles. The experimental data in Figure 12 indicate that Run 23 was not actually at steady-state and should have been continued longer. The data in Figure 13 (Run 24) indicate a slight deviation at 150 minutes and the reason for this is unknown. However, the other data from Run 24 appear to coincide quite closely with the double exponential model.

Runs 15 and 25 were completed under slightly different conditions than the other transient runs. Run 15 was completed at a 400°C adsorption temperature. Run 25 was completed at the lowest partial pressure ($P_{py} = 284 \text{ N/m}^2$). A simple indication of catalyst coking is the break in slope of the $\ln[(C_{pS})_{eq} - C_{pS}]/(C_{pS})_{eq}$ versus time plot as shown in Figures 7 and 9. When one straight line fits all the transient data, as is the case for Runs 15 and 25, the catalyst can be considered coke-free. The data from these runs coincide very well with the single exponential, reversible poisoning model which does not include coke terms. Figures 14 and 15 demonstrate this behavior.

The poisoning models demonstrate very accurate predictions of the experimental transient data. The relative error of the predicted data is less than 12% in all cases. This does not mean that more complicated pore diffusion models or even more complicated poison-coke models will not fit the data. However, these analytical expressions, which are

TABLE VIII
REVERSIBLE POISONING AND IRREVERSIBLE COKING MODEL PARAMETERS

Run	W_c (mg/g cat.)	β_1	β_2
15	*	-	-
17	2.849	4.67×10^{-3}	2.29×10^{-3}
22	3.800	5.74×10^{-3}	2.86×10^{-3}
23	3.942	1.22×10^{-2}	1.41×10^{-3}
24	2.847	2.24×10^{-2}	6.40×10^{-3}
25	*	-	-

* Runs 15 and 25 did not demonstrate coking behavior.

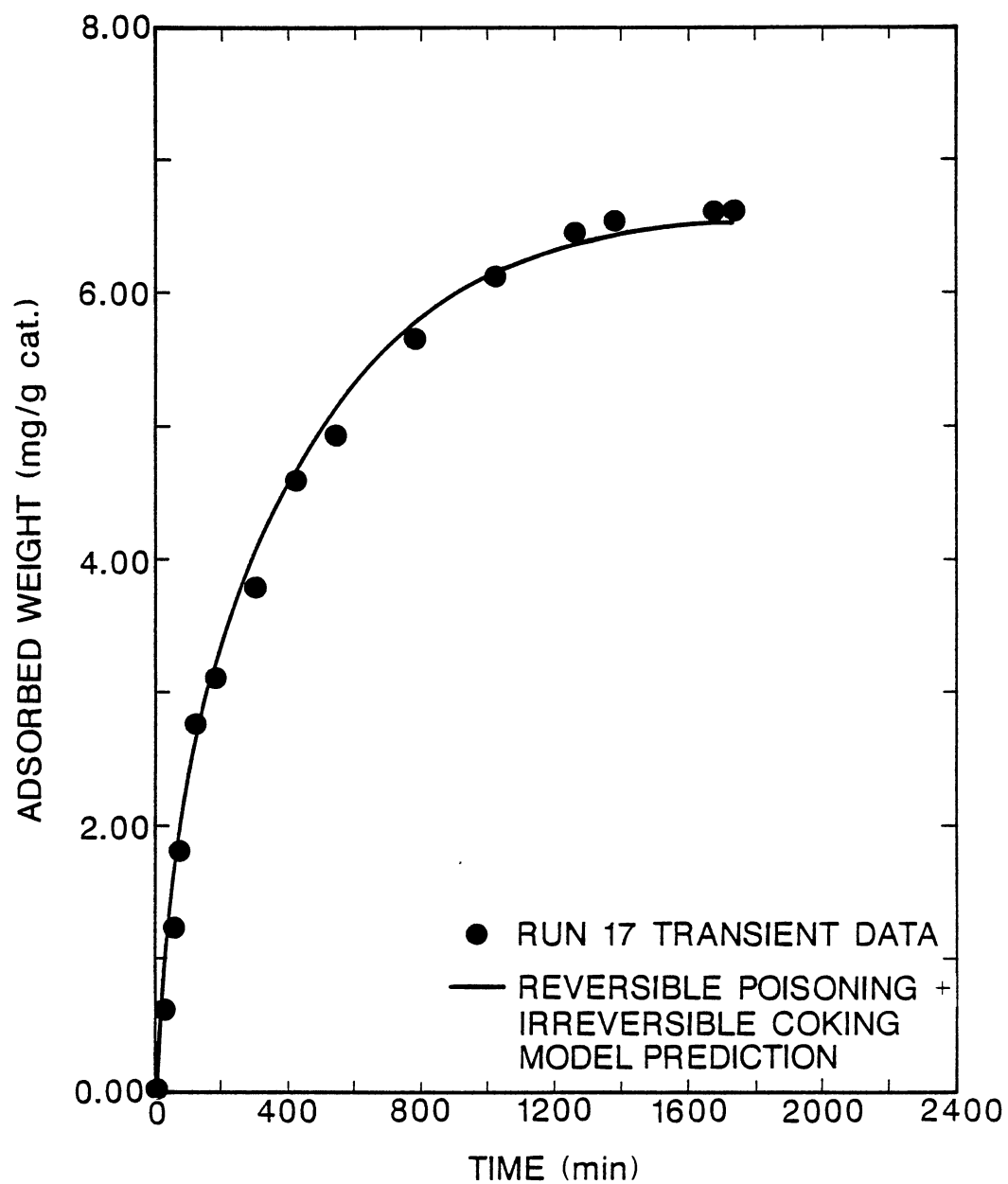


Figure 10. Run 17 Transient Adsorption Data Prediction from Reversible Poisoning and Irreversible Coking Models

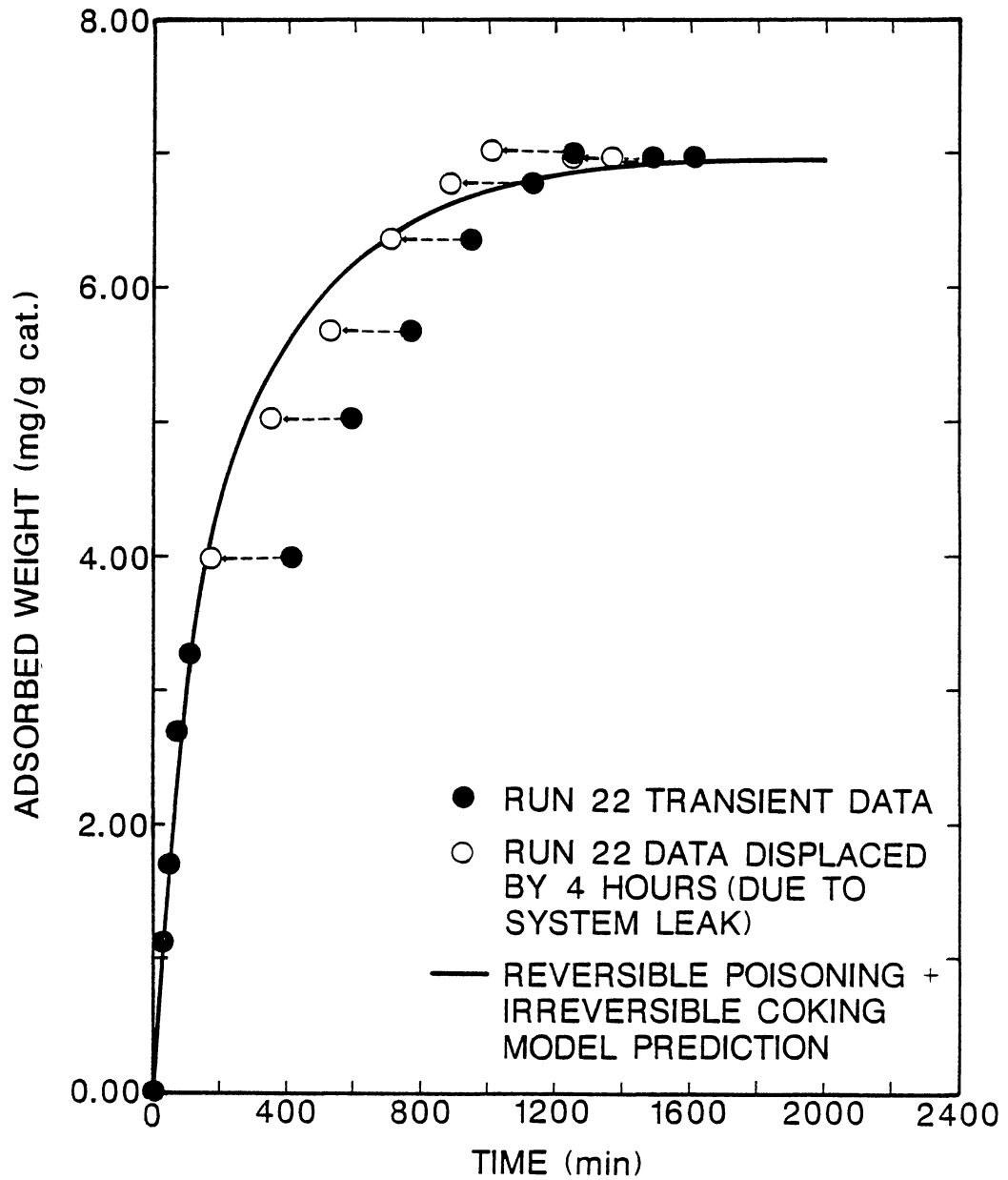


Figure 11. Run 22 Transient Adsorption Data Prediction from Reversible Poisoning and Irreversible Coking Models

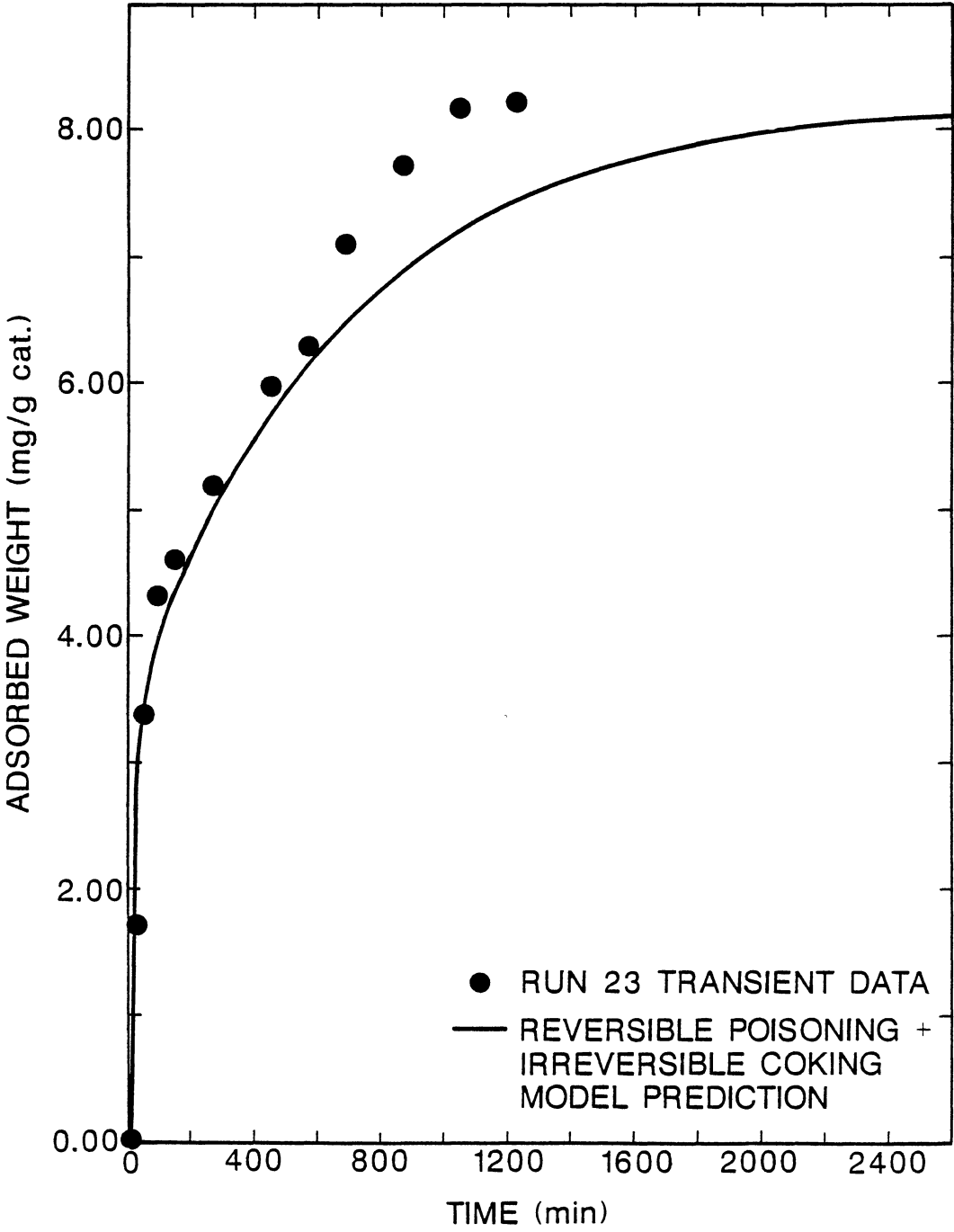


Figure 12. Run 23 Transient Adsorption Data Prediction from Reversible Poisoning and Irreversible Coking Models

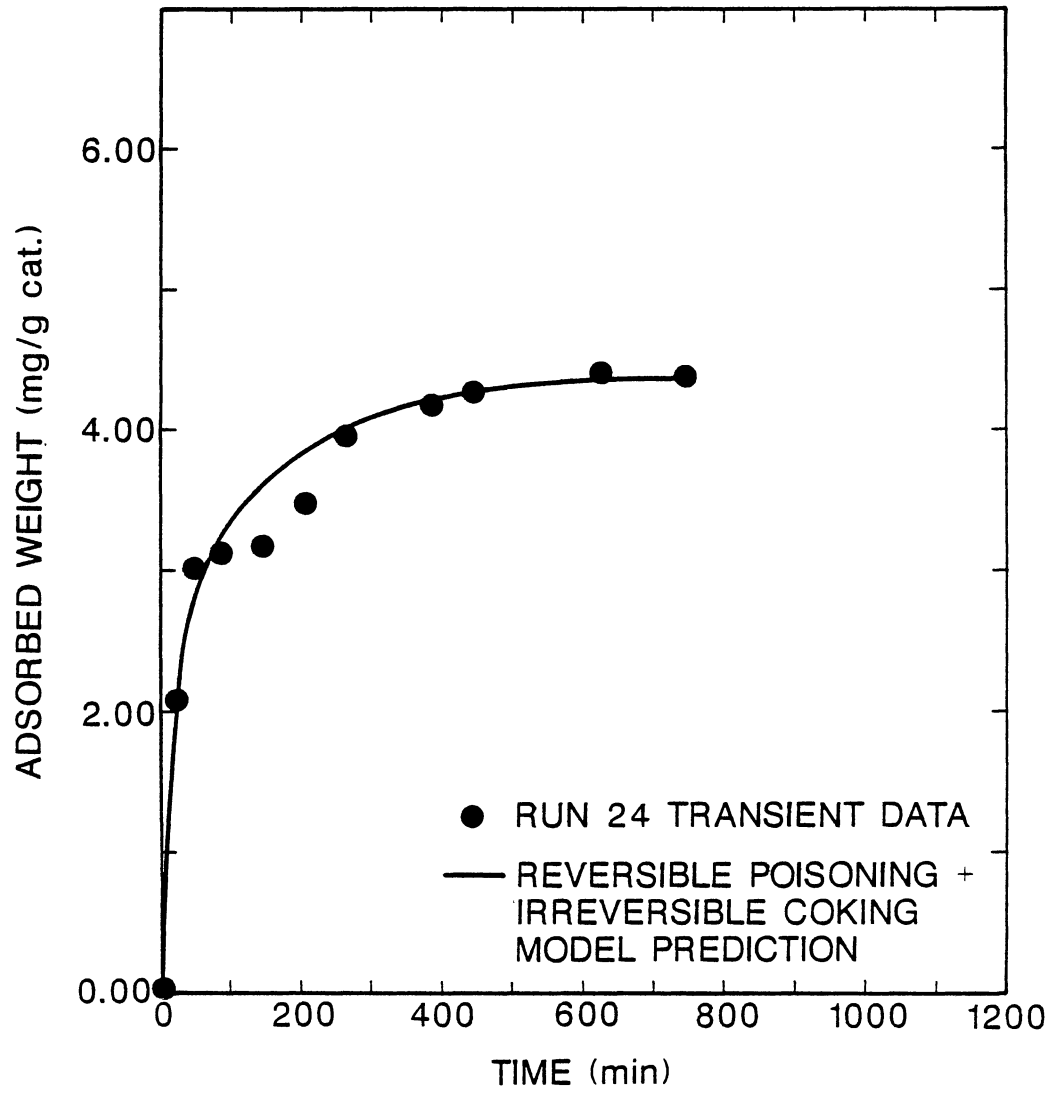


Figure 13. Run 24 Transient Adsorption Data Prediction from Reversible Poisoning and Irreversible Coking Models

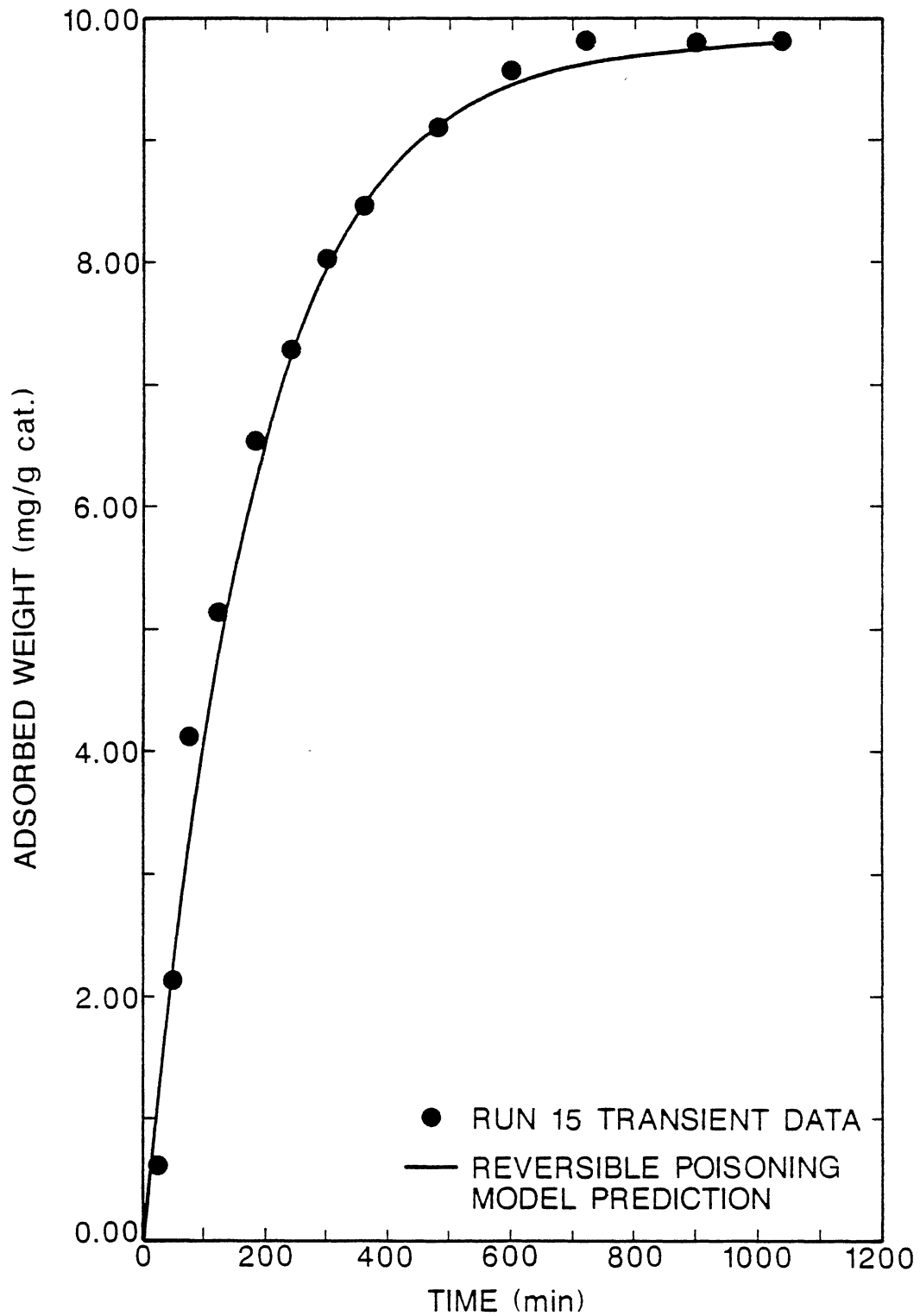


Figure 14. Run 15 Transient Adsorption Data Prediction from Reversible Poisoning Model

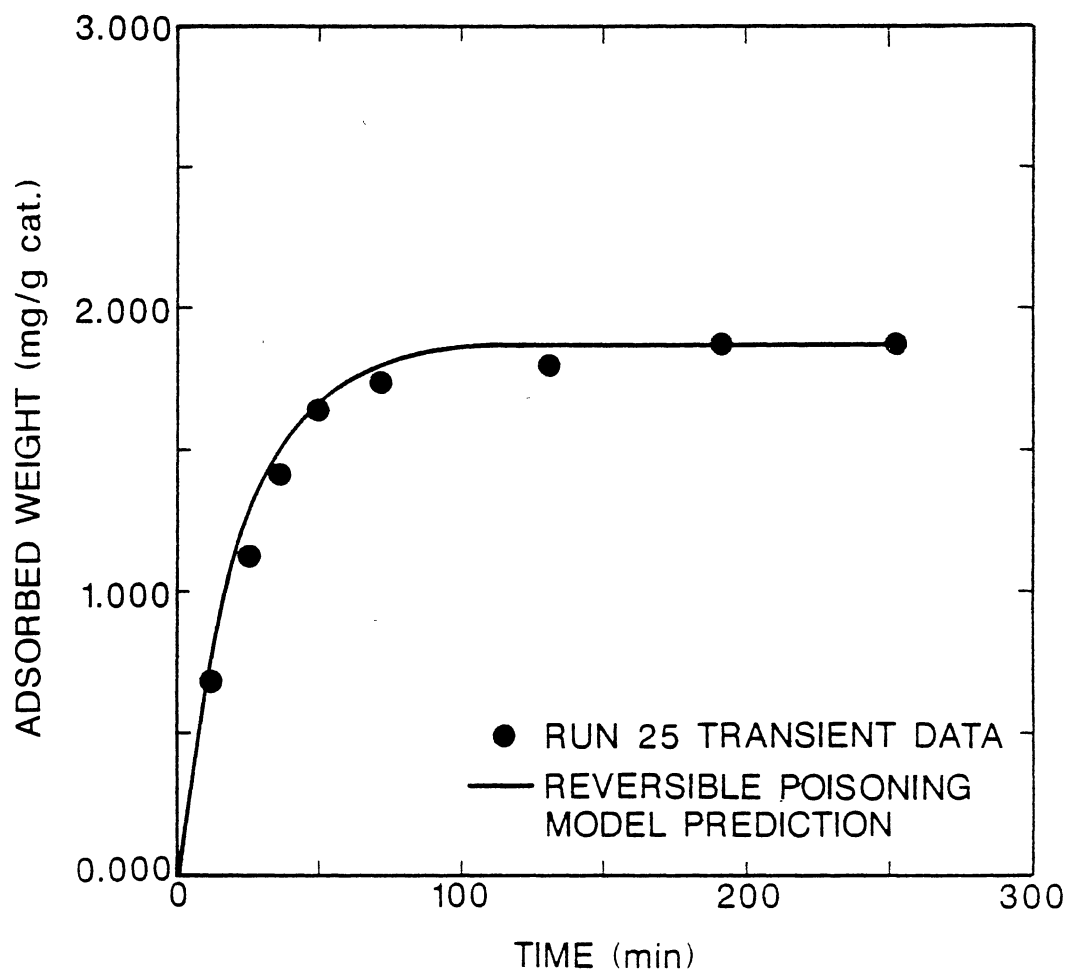


Figure 15. Run 25 Transient Adsorption Data Prediction from Reversible Poisoning Model

relatively simplistic, do a very adequate job with the type and amount of data collected in this experimental program.

One unexpected, but interesting, result was the catalyst reduction behavior. In the presence of hydrogen a catalyst in its oxidic form is expected to reduce (lose water as H_2O). The hydrogen reduction of the hydrotreating catalyst used in this experimentation is shown in Figure 4. With the catalyst made up of the compositions listed in Table II, one can expect 0.90 mg of oxygen to be available for reduction in the form of MoO_3 and NiO . 0.09 mg of oxygen are available as NiO and 0.81 mg of oxygen are available as MoO_3 . The data from Run 27 indicate 0.27 mg of weight reduction occurred. This suggests that all the NiO may have been reduced and part of the MoO_3 was reduced, the MoO_3 changed valence or some similar phenomena.

The unexpected result was the reduction of the catalyst by ammonia. For the ammonia reduction runs (Runs 26 and 28), 0.09 mg of oxygen were available on the catalyst as NiO and 0.85 mg oxygen were available as MoO_3 . The weight reduction was only 0.07 mg to 0.10 mg. This suggests that all or most of the NiO may have been reduced but the MoO_3 may not have been altered. There have been studies where ammonia was used as a titrant to study catalyst acidity and active sites (in the range of $400^\circ C$ to $600^\circ C$). To the best of my knowledge, there has not been any publication of ammonia reduction behavior and an explanation for it is unknown at this point. However, this type of result may be able to be used to study the effect that different catalyst preparation methods have on catalyst stability.

The reproducibility of the adsorption experiments is quite poor. Runs 19 and 21 demonstrate an attempt to reproduce $450^\circ C$ equilibrium

adsorption values at a pyridine partial pressure of 608 N/m^2 (see Table IV). An 87% difference exists between these two equilibrium values. The error in the adsorption data may be attributed to either the experimental sample or the experimental apparatus. Transient adsorption data for pyridine are demonstrated in Figure 3. The data do not demonstrate any erratic behavior which would indicate equipment sensitivity or disturbance problems. Furthermore, the experimental data do not demonstrate any dramatic deviations from the kinetic model predictions (shown in Figures 10-15). This observation further supports the theory that equipment variances did not contribute to experimental error.

The error in adsorption measurement must be attributed to sample deviations. Each adsorption experiment was completed with an individual catalyst extrudate and the probability that each catalyst demonstrated slightly different behavior is quite high. The sensitivity of the electrobalance allowed microgram differences in adsorption levels to be detected and any differences in catalyst behavior would be magnified by this sensitivity.

Two methods by which measurement errors due to sample standardization problems may be reduced are: 1) increase the sample size from one catalyst pellet to several pellets in order to eliminate adsorption comparisons of individual catalyst extrudates, and 2) increase the number of reproducibility experiments using a single catalyst pellet until the probability of collecting accurate data is increased. Utilization of either of these suggestions may reduce the data scatter which appears in the equilibrium adsorption isotherms (Figure 2).

CHAPTER VI

CONCLUSIONS AND RECOMMENDATIONS

There are several conclusions which can be made from the results of this pyridine poisoning study. These conclusions are:

1. Equilibrium adsorption isotherms for pyridine demonstrate idealized Langmuir characteristics (Type I isotherm behavior) in the partial pressure and temperature range used.
2. Equilibrium pyridine adsorption weight demonstrates a linear dependence on temperature.
3. Rate of poison deposition on the catalyst surface is very rapid during the initial 200 minutes of exposure.
4. There is no systematic trend between the transient adsorption data and partial pressure of the poison.
5. As adsorption temperature is decreased, the rate of adsorption and the equilibrium adsorption level both increase.
6. Pyridine adsorption at 450°C demonstrates a 33% irreversibility which is attributed to coke formation.
7. Some level of coke is forming on the catalyst surface and the coke level reaches a steady state.
8. Transient adsorption data is accurately described (relative error < 12%) by two, single exponential models. One model describes the

period when simultaneous reversible poisoning and irreversible coke formation is occurring on the catalyst surface. The other model describes the period when reversible poisoning is occurring on a catalyst which has attained a constant coke formation level. The two model parameters are functions of poison partial pressure and rate constants of adsorption, desorption, and coke formation.

9. When the Shell 324 catalyst is exposed to pure hydrogen the catalyst reduces.

10. When the Shell 324 catalyst is exposed to ammonia (in the same partial pressure and temperature range as that of pyridine) the catalyst reduces.

Several unexpected results were obtained during this experimental study and the following recommendations are made:

1. Collect adsorption data in the region where $P_p < 284 \text{ N/m}^2$ and calculate equilibrium constants and heat of adsorption.

2. Complete poison reversibility experiments at various temperatures and poison partial pressures.

3. Complete poison reversibility experiments about the point t_c . The region when $t < t_c$ should exhibit simultaneous reversible poisoning and irreversible coking. The region when $t > t_c$ should exhibit reversible poisoning only and maintain a constant coke level.

4. Test catalyst reducibility when exposed to various nitrogen compound bases and compare to both hydrogen and ammonia reduction.

5. Elucidate competitive adsorption effects between various nitrogen bases. Gas chromatography may allow surface concentrations of various components to be evaluated.

6. Complete poisoning studies on reduced catalysts as well as catalysts in the oxidic state.

7. Perform poisoning studies under conditions which more closely simulate industrial hydrotreatment processes.

8. Increase number of catalyst pellets used during adsorption experimentation in order to reduce adsorption measurement error.

BIBLIOGRAPHY

1. Tanabe, K.; "Solid Acids and Bases", New York: Academic Press, 1970.
2. Fu, C.; Schaffer, A. M.; Ind. Eng. Chem. Prod. Res. Dev., 24, 68 (1985).
3. Ward, J. W.; Advan. Chem. Ser., 101, 381 (1971).
4. Maxted, E. B.; Advan. Catalysis, 3, 129 (1951).
5. Pines, H.; Haag, W. O.; J. Amer. Chem. Soc., 82, 2471 (1960).
6. Mills, G. A.; Boedeker, E. R.; Oblad, A. G.; J. Amer. Chem. Soc., 72, 1554 (1950).
7. Hirschler, A. E.; J. Catal., 6, 1 (1966).
8. Takahashi, M.; Iwasawa, Y., Oga Sawara, S.; J. Catal., 45 15 (1976).
9. Cowley, S. W.; Massoth, F. E.; J. Catal., 51, 291 (1978).
10. Ramachandran, R.; Massoth, F. E.; Can. J. Chem. Eng., 60, 17 (1982).
11. Hall, W. K.; Schneider, R. L.; Valyon, J.; J. Catal., 85, 277 (1984).
12. McIlvried, H. G.; Ind. Eng. Chem. Proc. Des. Dev., 10(1), 25 (1971).
13. Entz, R. W.; M. S. Thesis, Oklahoma State University, Stillwater, Oklahoma, (1984).
14. Satterfield, C. N.; Cocchetto, J. F.; AIChE J., 21(6), 1107 (1975).
15. Satterfield, C. N.; Modell, M.; Mayer, J.; AIChE J., 21(6), 1100 (1975).
16. Shih, S.; Reiff, E.; Zawadzki, R.; Katzer, J. R.; Amer. Chem. Soc., Prepr., 23, 99 (1978).
17. Goudriaan, F.; Gierman, H.; Vlugter, J. C.; J. Inst. Pet., 59(565), 40 (1973).

18. Thakkar, V. P.; Baldwin, R. M.; Bain, R. L.; Fuel Proc. Tech., 4, 235 (1981).
19. Anderson, R. B.; Whitehouse, A. M.; Ind. Eng. Chem., 53(12), 1011 (1961).
20. Ozawa, Y.; Bischoff, K. B.; Ind. Eng. Chem. Proc. Des. Dev., 7(11), 67 (1968).
21. Dumez, F. J.; Froment, G. F.; Ind. Eng. Chem. Proc. Des. Dev., 15(2), 291 (1976).
22. Krishnaswamy, S.; Kittrell, J. R.; Ind. Eng. Chem. Proc. Des. Dev., 18(3), 399 (1979).
23. Romero, A.; Bibao, J.; Gonzalez-Velasco, J. R.; Ind. Eng. Chem. Proc. Des. Dev., 20, 570 (1981).
24. Nam, I.; Kittrell, J. R.; Ind. Eng. Chem. Proc. Des. Dev., 23, 237 (1984).
25. Takeuch, M.; Ishige, T.; Fukumuro, T.; Kubota, H.; Shimdo, M.; Kagaku Kogaku, 4, 387 (1966).
26. Chang, H. J.; Seapan, M.; Crynes, B. L.; "Chemical Reaction Engineering - Boston," ACS Symposium Series, 196, 1982.
27. Smith, J. M.; "Chemical Engineering Kinetics, 3rd Ed.", New York: McGraw-Hill Book Company, 1981, p. 363.

APPENDIX A
BUOYANCY CALCULATIONS

APPENDIX A

BUOYANCY CALCULATIONS

As the concentration of poison in the TGA feed is increased, one may expect buoyancy to have an effect on the adsorbed weight results. This potential problem will be investigated in this Appendix.

The volume of the solid catalyst is given as the void volume due to pores subtracted from the total cylindrical volume:

$$V_{\text{solid}} = V_{\text{total}} - V_{\text{void}}$$

The reduction of weight due to density differences is given by:

$$\text{reduction} = (\rho_{\text{g}} - \rho_{\text{He}}) V_{\text{solid}}$$

where,

ρ_{g} \equiv density of poison gas at system conditions, mass /volume.

ρ_{He} \equiv density of He gas at system conditions, mass/volume.

Volume calculations are given as follows:

$$V_{\text{total}} = \frac{\pi D^2 L}{4} = \pi \frac{(1/16 \text{ in})^2 (1/4 \text{ in})}{4} \left(\frac{2.54 \text{ cm}}{\text{in}}\right)^3 = 0.01257 \text{ cm}^3$$

$$V_{\text{void}} = \left(\frac{0.50 \text{ cm}^3}{\text{g cat.}}\right) (\text{x g cat.}) = 0.5 \text{ x cm}^3$$

$$V_{\text{solid}} = [0.01257 - 0.5 \text{ x}] \text{ cm}^3$$

Density calculations are given as follows:

$$\rho = \frac{MP}{RT} = \frac{m}{v}$$

$$\rho_{\text{He}} = \frac{(4 \text{ g/gmol}) (1 \text{ atm})}{(82.05 \frac{\text{l atm}}{\text{g mol K}}) (450 + 273) \text{K}} = 6.74 \times 10^{-5} \text{ g/l}$$

$$M_{\text{He-Py}} = \frac{(4) (\% \text{He}) + 79 (\% \text{Py})}{100}$$

$$\rho_{\text{He-Py}} = \frac{(M_{\text{He-Py}}) (1 \text{ atm})}{(82.05 \frac{\text{l atm}}{\text{g mol K}}) (450 + 273) \text{K}} = y \text{ g/l}$$

$$\text{Wt. change} = (\rho_{\text{He-Py}} - \rho_{\text{He}}) V_{\text{solid}}$$

$$= (y - 6.74 \times 10^{-5}) \frac{\text{g}}{\text{l}} \left(\frac{1 \text{ l}}{0.3532 \text{ ft}^3}\right) \left(\frac{\text{in}}{2.54 \text{ cm}}\right)^3 \left(\frac{\text{ft}}{12 \text{ in}}\right)^3$$

$$(0.1257 - 15\text{x}) \text{ cm}^3 \left(\frac{\text{mg}}{10^{-3} \text{ g}}\right)$$

$$= (y - 6.74 \times 10^{-5}) (.01257 - .5\text{x}) \text{ mg}$$

Table IX lists all the appropriate buoyancy parameters and indicates that buoyancy does not affect the data at the concentrations in this experimentation.

TABLE IX
 BUOYANCY CHANGES IN EQUILIBRIUM PYRIDINE ADSORPTION DATA

Run	Temp. (°C)	Cat. Wt. (mg)	P_{py} (N/m ²)	Ads. Wt. (mg/g cat.)	Buoyancy Change (mg/g cat.)
15	400	11.4119	1110	9.814	1.5×10^{-4}
	350			12.269	2.1×10^{-4}
	250			20.154	2.5×10^{-4}
17	450	13.1218	1620	6.630	1.7×10^{-4}
19	450	8.5859	608	2.574	1.3×10^{-4}
21	450	12.1720	608	1.360	7.2×10^{-5}
	350			10.598	8.9×10^{-5}
	250			20.703	1.1×10^{-4}
22	450	15.9919	1220	6.979	7.0×10^{-5}
	350			11.131	8.4×10^{-5}
	250			13.263	1.0×10^{-4}
23	450	11.1750	2130	8.217	2.4×10^{-4}
	350			12.989	2.8×10^{-4}
	250			19.596	3.4×10^{-4}

TABLE IX (Continued)

Run	Temp. (°C)	Cat. Wt. (mg)	P_{py} (N/m ²)	Ads. Wt. (mg/g cat.)	Buoyancy Change (mg/g cat.)
24	450	12.5560	1820	4.380	1.14×10^{-5}
	350			10.067	1.87×10^{-5}
	250			17.044	2.87×10^{-5}
25	450	10.9435	284	1.873	2.31×10^{-6}
	350			11.742	9.70×10^{-6}
	250			19.336	1.99×10^{-5}

APPENDIX B

PROGRESSIVE SHELL MODEL DERIVATION

APPENDIX B

PROGRESSIVE SHELL MODEL DERIVATION

If the adsorption reaction causing poisoning is very fast, the outer part of a catalyst pellet will be completely deactivated, while the central portion retains its unpoisoned activity. In this type of poisoning a layer of poisoned catalyst will start to grow on the outer catalyst surface and gradually move as a function of time to the center of the catalyst. In the extreme case the boundary between the deactivated and active catalyst will remain sharply defined during the deactivation process. This type of poisoning is called a progressive shell model.

Smith (27) has derived a relation between the fraction of a catalyst surface which has been poisoned, α , and time. This expression is given by:

$$\frac{d\alpha}{dt} = \frac{k_p}{n_0} C_p (1 - \alpha)$$

where,

α \equiv fraction of catalyst surface which is poisoned, n/n_0 .

n_0 \equiv adsorbed concentration corresponding to complete deactivation (monolayer coverage of poison), mass/g cat.

t \equiv time, min.

k_p \equiv first order adsorption rate constant, min^{-1} volume/mass.

C_p \equiv fluid phase concentration of poison, mass/volume.

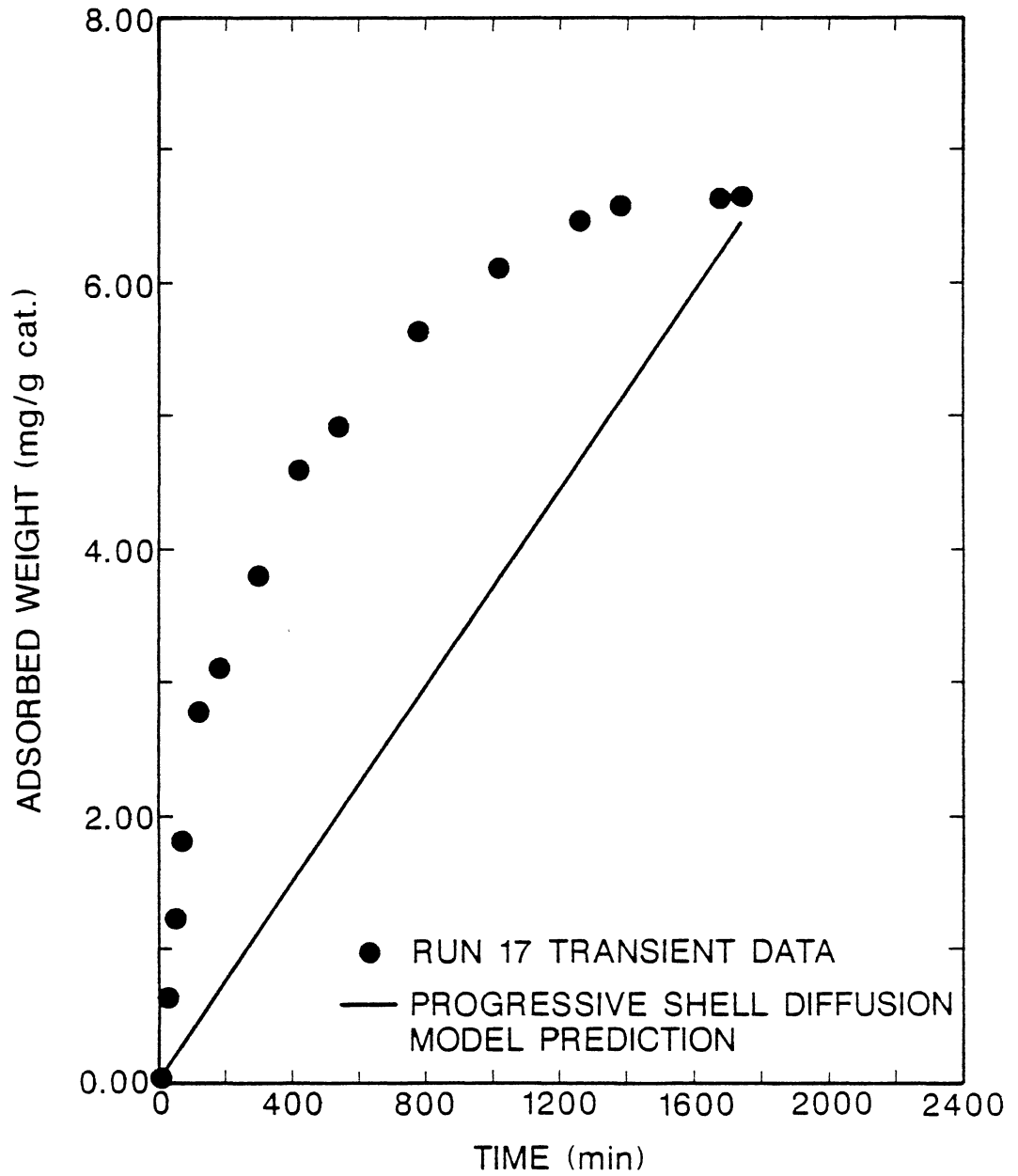


Figure 16. Run 17 Transient Adsorption Data Prediction from Progressive Shell Model

However, examine some of the assumptions used in deriving Equation (i) and compare them to the poisoning mechanism.

The most important simplifying assumption is that the rate of the adsorption reaction is an irreversible, first order reaction given by: $r = k_p C_p (1 - \alpha)$. However, the poisoning mechanism is believed to be a reversible process where the rate of adsorption is given by $r = k_a P_p C_S - k_d C_p S$. The second assumption is that the poison adsorption reaction is assumed to be rapid enough that a distinct boundary exists between the active and deactivated portions of the catalyst. Whether or not this is a good assumption is unknown, but it probably is too simplistic.

Simple analytical expressions are always preferred over complex models. However, in the case of a progressive shell model, the data fit is quite poor. In order to better describe the data one must incorporate more realistic behavior (e.g., a reversible poisoning reaction). This dramatically complicates the mathematics of a progressive shell model. On the other hand, the kinetic expressions derived in Chapter V are not only simple analytical expressions, but they fit the data well and account for realistic behavior (i.e. reversible poisoning, irreversible coking, etc.).

APPENDIX C

REDUCTION CALCULATIONS

APPENDIX C

REDUCTION CALCULATIONS

The hydrogen reduction experiment was completed in Run 27. In order to calculate the total amount of oxygen available for reduction use the following:

$$\left[\frac{2.67 \text{ mg Ni}}{100 \text{ mg cat.}} \times \frac{15.999 \text{ mg O}}{58.70 \text{ mg Ni}} \right] + \frac{13.05 \text{ mg Mo}}{100 \text{ mg cat.}} \times \frac{47.997 \text{ mg O}}{95.94 \text{ mg Mo}} \left[12.399 \text{ mg cat.} \right] = 0.90 \text{ mg O}$$

0.09 mg O available from NiO

0.81 mg O available from MoO₃

However, the total amount of weight loss which was noticed was 0.27 mg.

The same calculation can be made for the ammonia reduction experiments and the results are shown in Table IV.



VITA

Jeffrey Alan Kittrell

Candidate for the Degree of
Master of Science

Thesis: EQUILIBRIUM AND TRANSIENT PYRIDINE POISONING OF A HYDROTREATING CATALYST

Major Field: Chemical Engineering

Biographical:

Personal Data: Born in Wilmington, Delaware, August 11, 1962, the son of Dr. James R. and Georgia Ruth Kittrell.

Education: Graduated from Amherst Regional High School, Amherst, Massachusetts in June, 1980; received a Bachelor of Science degree in Chemical Engineering from Michigan State University in August, 1984; completed requirements for the Master of Science degree in Chemical Engineering at Oklahoma State University in May, 1986.

Professional Experience: Graduate Teaching/Research Assistant, School of Chemical Engineering, Oklahoma State University, Stillwater, Oklahoma, 8/84-1/86; Research Engineer, K.S.E., Inc., Sunderland, Massachusetts, 6/83-9/83; accepted employment as Process Engineer with Chevron U.S.A., Port Arthur, Texas, 2/86; First Prize Award, 1984 AIChE - Environmental Division Undergraduate Student Paper Contest; 1985 Recipient - Amoco Foundation Master's Fellowship; member AIChE and Omega Chi Epsilon.